



Title	Freezing, Melting, and Light Stress on the Photophysiology of Ice Algae: Ex Situ Incubation of the Ice Algal diatom <i>Fragilariopsis cylindrus</i> (Bacillariophyceae) Using an Ice Tank
Author(s)	Yoshida, Kazuhiro; Seger, Andreas; Kennedy, Fraser; McMinn, Andrew; Suzuki, Koji
Citation	Journal of Phycology, 56(5), 1323-1338 <a href="https://doi.org/10.1111/jpy.13036">https://doi.org/10.1111/jpy.13036</a>
Issue Date	2020-10
Doc URL	<a href="http://hdl.handle.net/2115/82871">http://hdl.handle.net/2115/82871</a>
Rights	This is the peer reviewed version of the following article: Yoshida, K. Seger, A. Kennedy, F. McMinn, A. Suzuki, K. Freezing, Melting, and Light Stress on the Photophysiology of Ice Algae: Ex Situ Incubation of the Ice Algal diatom <i>Fragilariopsis cylindrus</i> (Bacillariophyceae) Using an Ice Tank. Journal of Phycology. 2020; 56(5): 1323-1338, which has been published in final form at <a href="https://doi.org/10.1111/jpy.13036">https://doi.org/10.1111/jpy.13036</a> . This article may be used for non-commercial purposes in accordance with Wiley Terms and Conditions for Use of Self-Archived Versions.
Type	article (author version)
Additional Information	There are other files related to this item in HUSCAP. Check the above URL.
File Information	Yoshida et al. Accepted_JPhycol.pdf



[Instructions for use](#)

1 FREEZING, MELTING AND LIGHT STRESS ON THE PHOTOPHYSIOLOGY OF  
2 ICE ALGAE: *EX SITU* INCUBATION OF THE ICE ALGAL DIATOM  
3 *FRAGILARIOPSIS CYLINDRUS* (BACILLARIOPHYCEAE) USING AN ICE TANK<sup>1</sup>

4

5 Kazuhiro Yoshida

6 Graduate School of Environmental Science, Hokkaido University, North 10 West 5,

7 Kita-Ku, Sapporo, Hokkaido 060-0810 Japan

8 Institute for Marine and Antarctic Studies, University of Tasmania, 20 Castray

9 Esplanade, Battery Point TAS 7004 Australia

10

11 Andreas Seger

12 Institute for Marine and Antarctic Studies, University of Tasmania, 20 Castray

13 Esplanade, Battery Point TAS 7004 Australia

14 South Australian Research and Development Institute, 2b Hartley Grove, Urrbrae, SA,

15 5064 Australia

16

17

Fraser Kennedy, Andrew McMinn<sup>2</sup>

18

Institute for Marine and Antarctic Studies, University of Tasmania, 20 Castray

19

Esplanade, Battery Point TAS 7004 Australia

20

21

and Koji Suzuki

22

Faculty of Environmental Earth Science, Hokkaido University, North 10 West 5, Kita-

23

Ku, Sapporo, Hokkaido 060-0810 Japan

24

25 <sup>1</sup> Submitted 24/06/2019

26 <sup>2</sup> Author for correspondence:

27 Andrew McMinn

28 Tel: +61- 3 6226 6379

29 E-mail: Andrew McMinn@utas.edu.au

30

31 RUNNING HEAD: Ice algal physiology in an ice tank

32

33 KEYWORDS: active chl *a* fluorescence; algal pigments; ice tank incubation;

34 photoprotection; *psbA*; *rbcL*; sea ice

35

36 ABBREVIATIONS:

37 cDNA, complementary DNA; Chl *a*, chlorophyll *a*; ChlF, active chlorophyll *a*

38 fluorescence; DD, diadinoxanthin; DT, diatoxanthin; DES, de-epoxidation state index

39 of DD-DD xanthophyll cycle; ETR, electron transport rate; Fe<sup>'</sup>, inorganic Fe species;

40 FRRf, fast repetition rate fluorometry; HL, high light; LL, low light; NPQ, non-

41 photochemical quenching; PQ, plastoquinone; *PP*, primary productivity; PPC,

42 photoprotective carotenoid; PSC, photosynthetic carotenoid; Q<sub>A</sub>, the first quinone

43 electron acceptor; Q<sub>B</sub>, secondary quinone electron acceptor; Tchl *a*, total chl *a*;

44 UHPLC, ultra-high performance liquid chromatography

45

46 ABSTRACT

47 Sea-ice algae contribute up to 25% of the primary productivity of polar seas and seed  
48 large-scale ice-edge blooms. Fluctuations in temperature, salinity, and light associated  
49 with the freeze/thaw cycle can significantly impact the photophysiology of ice-  
50 associated taxa. The effects of multiple co-stressors (i.e., freezing temperature and high  
51 brine salinity or sudden high light exposure) on the photophysiology of ice algae were  
52 investigated in a series of ice tank experiments with the polar diatom *Fragilariopsis*  
53 *cylindrus* under different light intensities. When algal cells were frozen into the ice, the  
54 maximum quantum yield of photosystem II photochemistry (PSII) ( $F_v/F_m$ ) decreased  
55 possibly due to the damage of PSII reaction centres and/or high brine salinity stress  
56 suppressing the reduction capacity downstream of PSII. Expression of the *rbcL* gene  
57 was highly upregulated, suggesting that cells initiated strategies to enhance survival  
58 upon freezing in. Algae contained within the ice-matrix displayed similar levels of  
59  $F_v/F_m$  regardless of the light treatments. Upon melting out, cells were exposed to high  
60 light ( $800 \mu\text{mol photons m}^{-2} \text{s}^{-1}$ ), resulting in a rapid decline in  $F_v/F_m$  and significant  
61 upregulation of non-photochemical quenching (NPQ). These results suggest that ice  
62 algae employed safety valves (i.e., NPQ) to maintain their photosynthetic capability  
63 during the sudden environmental changes. Our results infer that sea ice algae are highly  
64 adaptable when exposed to multiple co-stressors and that their success can, in part, be

- 65 explained by the ability to rapidly modify their photosynthetic competence; a key factor
- 66 contributing to algal bloom formation in the polar seas.

67 INTRODUCTION

68 Sea ice algae are significant primary producers in sea ice zones. They contribute  
69 5–25% of the total primary production (*PP*) in seasonally ice-covered regions  
70 (Legendre et al. 1992, Lizotte 2001, Michel et al. 2006, Loose et al. 2011, Arrigo 2017)  
71 and ~50% of the annual *PP* in perennially ice-covered regions (Satoh et al. 1989,  
72 McMinn et al. 2010, Fernandez-Mendez et al. 2015). Ice-associated algae are of high  
73 ecological importance as not only the primary energy source for sea ice biota such as  
74 zooplankton, krill, larval fish and benthos (Lizotte 2001, Boetius et al. 2013, 2015,  
75 Kohlbach et al. 2017, Moteki et al. 2017, Bernard et al. 2018) but also as seed biomass  
76 for ice-edge blooms in marginal sea ice zones (e.g., Smith and Nelson 1986, Syvertsen  
77 1991, Arrigo and van Dijken 2003, Arrigo 2014). Ice-edge blooms, which ice algae may  
78 seed, contribute ~50% of the total *PP* in marginal sea ice zone of the Southern Ocean  
79 (Smith and Nelson 1986, Sakshaug and Slagstad 1991, Deppeler and Davidson 2017),  
80 although it is still controversial which ice algae or phytoplankton actually contribute to  
81 the blooms (see review of van Leeuwe et al. 2018). Upon freezing in, algae can form  
82 aggregates within microstructures of the ice, which channel excluded liquid brine from  
83 sea ice to under-ice seawater when ice grows (i.e., brine channels) (Melnikov and  
84 Bondarchuk 1987, Assmy et al. 2013, Boetius et al. 2013, Katlein et al. 2015,

85 Fernandez-Mendez et al. 2014, Boetius et al. 2015). During the sea ice melt, these algal  
86 aggregates can rapidly sink and transport carbon down to the sea floor. This process  
87 contributes to the biological carbon pump (Riebesell et al. 1991, Taguchi et al. 1997,  
88 Boetius et al. 2013, Katlein et al. 2015) and underlines the important contribution of ice  
89 algae to both the ecology and biogeochemistry of sea ice zones. It is thus important to  
90 understand how ice algae survive in the dynamic and heterogeneous sea ice  
91 environment. Sea ice environments are subject to large fluctuations in temperature  
92 ( $\sim -20$  °C to  $-1.8$  °C; Petrich and Eicken 2017), salinity ( $\sim 25$  to 170; Arrigo et al. 2010)  
93 and light availability ( $\sim 0$  to  $1000 \mu\text{mol photons m}^{-2} \text{ s}^{-1}$ ; Galindo et al. 2017). Variation  
94 in these abiotic parameters can influence the photosynthetic efficiency of ice algae,  
95 however, they are not independent (i.e. multiple co-stressors; McMinn et al. 2017). Few  
96 studies have addressed the influence of multiple co-stressors on the photophysiology of  
97 sea ice algae (Ralph et al. 2005, 2007, Ryan et al. 2011, Martin et al. 2011, McMinn et  
98 al. 2014; see review of McMinn 2017), and little is known about how co-stressors  
99 influence ice algal photosynthesis and production during freeze/thaw cycles (McMinn  
100 2017). Despite their significant ecological and biogeochemical importance, it remains  
101 difficult to directly obtain the photophysiological properties of sea ice taxa *in situ*.  
102 Kennedy et al. (2012) were the first to use sea ice tanks to undertake short-term

103 incubation of the haptophyte *Phaeocystis antarctica* within the laboratory. This method  
104 has the advantage that ice algae can be incubated in an environment mimicking pack ice  
105 conditions. Although many studies have addressed ice algal photosynthesis and  
106 production using isolates resuspended in water (e.g., Yan et al. 2019), it remains  
107 difficult to incubate them in the laboratory (e.g. in a culturing flask), while simulating  
108 realistic environmental conditions. Using a previous ice tank model, Kennedy et al.  
109 (2012) found that a freezing event suppressed the photochemical efficiency of PSII.  
110 Although these experiments were able to reveal the effects of freezing on the  
111 photophysiology of ice algae, their short-term nature did not address the longer-term  
112 mechanism of freezing stress. Understanding how ice algae maintain photosynthetic  
113 capacity and survive during freeze/thaw cycles is of considerable importance to better  
114 assess primary productivity in sea ice environments. In this study, a novel 70 L ice tank  
115 was constructed for the long-term incubation of ice algae under ecologically realistic  
116 conditions. It was used to investigate the effects of multiple co-stressors on ice algal  
117 photophysiology:

- 118 (1) freezing stress with low temperature and high brine salinity;
- 119 (2) chronic low light availability under low temperature and high salinity;

120 (3) melting stress with exposure to less saline meltwaters and sudden increase in light.

121 The sea ice diatom *Fragilariopsis cylindrus* was maintained in the ice tank for 20 days  
122 followed by ice melt and light exposure experiments to reproduce the environment that  
123 released ice algae experience. This study aims to investigate the effects of multiple co-  
124 stressors on ice algal photophysiology in an artificial sea ice environment during a  
125 freeze/thaw cycle. It provides new insights into how ice algae are able to tolerate  
126 environmental fluctuations that contribute to their dominance of ice-edge blooms.

127

## 128 MATERIALS AND METHODS

### 129 *Ice tank incubation*

130 The polar pennate diatom *Fragilariopsis cylindrus* (isolated from Antarctic sea ice in  
131 2015, Davis station, East Antarctica; Kennedy et al. 2019), was incubated in a purpose  
132 designed ice tank (Island Research, Tasmania). The algal culture was less than two  
133 years old at the start of the experiments. The ice tank was contained within a freezer (–  
134 20 °C), and the ice thickness and temperature gradient of the ice were controlled by  
135 interactions between a basal heater and the adjustable ambient freezer temperature (Fig.  
136 1). This enabled an ice thickness of approximately 5.5 cm to be maintained during the  
137 experiment. *F. cylindrus* was incubated in Aquil media (Price et al. 1989), buffered with

138 ethylenediaminetetraacetic acid (EDTA) (final concentration 5.00  $\mu\text{M}$ ) at a salinity of  
139 35, and a Fe concentration of 400 nM. The concentration of total inorganic forms of Fe  
140 ( $\text{Fe}^{\text{'}}$ ) was 1.54 nM, this being continuously supplied from the Fe-EDTA complexes to  
141 the medium calculated using the software Visual MINTEQ, ver. 3.1  
142 (<https://vminteq.lwr.kth.se>). Light intensities beneath the ice, measured with a spherical  
143 photosynthetically active radiation (PAR) sensor (QSL-100, Biospherical Instrument  
144 Inc.), were set at 150 and 30  $\mu\text{mol photons m}^{-2} \text{s}^{-1}$  (White LED, PANEL-300-18W,  
145 LED Lighting Products, Australia; Fig. S1) as high and low light (HL and LL)  
146 treatments, respectively. Two discrete ice tank runs were conducted for each light  
147 treatment. The diatom *F. cylindrus* was inoculated with low cell densities (HL:  $4011 \pm$   
148  $151 \text{ cells mL}^{-1}$ ; LL:  $3933 \pm 132 \text{ cells mL}^{-1}$ ) to avoid the possibilities of self-shading  
149 and nutrient starvation during the incubation experiments. They were maintained in the  
150 ice tank for 3 days for acclimation where seawater temperature was maintained at 2.5  
151  $^{\circ}\text{C}$ . Prior to freezing in, a sample was taken to assess the original physiological state of  
152 the algae (day -05, hereafter). The temperature lowered to  $-1.8 \text{ }^{\circ}\text{C}$  to initiate ice  
153 formation. Once ice had formed after 3 days, the under-ice water was partially replaced  
154 with ultrapure water to reduce the salinity down to 35; as the salinity of the underlying  
155 water had increased (to  $\sim 38$ ) as a result of brine rejection. Two-day acclimation period

156 was used prior to sampling. Ice sampling was conducted every 5 days for 20 days (days  
157 00, 05, 10, 15, and 20). Brine salinity and brine fraction were estimated following Cox  
158 and Weeks (1983) and Eicken (2009). To minimize heterogeneity among ice cores, ice  
159 samples were randomly collected from the tank chamber (pseudo-replicate) with a trace  
160 metal-free hand drill (2 cm in diameter) from randomly annotated grids on the ice  
161 surface, following normal random sampling numbers generated by the software R  
162 (<https://www.r-project.org/>). To assess both the effects of melting and high light  
163 exposure, ice samples were melted at 2.5 °C and salinity 25 for 2 days (melt samples,  
164 hereafter). The melt samples were then exposed to intense light (light samples,  
165 hereafter) ( $800 \mu\text{mol photons m}^{-2} \text{s}^{-1}$ ) to mimick the typical summer surface  
166 (MODIS/Aqua).

167

#### 168 *Fast repetition rate (FRR) fluorometry*

169 To monitor the photophysiology of *F. cylindrus* during the freezing and melting  
170 processes, variable chlorophyll *a* fluorescence (ChlF) measurements were conducted  
171 using a bench-top Fast Repetition Rate fluorometer (FRRf) (FastOcean Act2Run  
172 Systems, Chelsea Technologies) with Act2Run software (Chelsea Technologies).  
173 Thawed ice samples were buffered with filtered seawater (ice:seawater ratio = 1: 1) at

174 2.5 °C in the dark for 30 min, and the slushy melted ice samples were placed in a quartz  
175 cuvette to measure fluorescence. A single turnover protocol was applied for ChlF  
176 measurement; 100 flashlets with 1 μs duration at a wavelength 450 nm and 2 μs  
177 intervals for excitation of reaction centres of PSII and 20 flashlets with 1 μs duration  
178 and 20 flashlets with 1 μs duration and 100 μs intervals for relaxation. Eighteen light  
179 steps were applied to generate a rapid light curve (RLC) from 0 to 800 μmol photons  
180 m<sup>-2</sup> s<sup>-1</sup>, taking <5 min to complete one RLC. At each light step (~15 s), at least five  
181 induction and relaxation curves were averaged to obtain ChlF yields, described in Table  
182 1, after calibrating the ChlF yields with filtered seawater. According to the models  
183 proposed by Kolber et al. (1998), photosynthetic parameters of chlorophyll *a* (chl *a*)  
184 induction curves were calculated based on the ChlF yields as shown in Table 1. Electron  
185 transport rate through the reaction centres of PSII (RCII) (ETR<sub>RCII</sub>) was calculated as  
186 follows:

188 
$$\text{ETR}_{\text{RCII}} = E \times \sigma_{\text{PSII}} \times \frac{F'_q/F'_m}{F_v/F_m} \times \Phi_{\text{RCII}} \times 6.022 \times 10^{-1}$$

187

189 following Suggett et al. (2011) and Schuback et al. (2016), an alternative approach to  
190 calculating ETR<sub>RCII</sub> of Kolber et al. (1998), wherein Φ<sub>RCII</sub> is the quantum yield of RCII

191 assumed as 1, and the following number is a conversion factor to mol quanta mol  
192  $\text{RCII}^{-1} \text{ s}^{-1}$ . The calculated  $\text{ETR}_{\text{RCII}}$  at each light step were fitted to the model of Platt et  
193 al. (1980) to obtain photosynthesis–irradiance ( $\text{ETR}_{\text{RCII}}-E$ ) parameters (Table 1). To  
194 assess the heat dissipation of algal cells, non-photochemical quenching based on the  
195 normalized Stern-Volmer (S-V) coefficient ( $\text{NPQ}_{\text{NSV}}$ ) under the actinic light equivalent  
196 to the incubation light intensities was also calculated following McKew et al. (2013):

197 
$$\text{NPQ}_{\text{NSV}}' = F_o' / F_v'$$

198

199 where  $F_o'$  is a minimum ChlF yield after a relaxation sequence calculated following  
200 Oxborough and Baker (1997) (Table 1).

201

202 *Validation experiments of melting procedures of ice samples for ChlF measurement*

203 While ChlF has been widely used on seawater samples (e.g., Suggett et al. 2011), it  
204 has not been broadly applied to ice algae research (Miller et al. 2015) because of the  
205 need for the ice samples to be melted. Melting the ice samples changes the  
206 photophysiology of the algal cells (e.g., Garrison and Buck 1986, Mikkelsen and  
207 Witkowski 2010, Rintala et al. 2014, Campbell et al. 2019). Here, multiple comparisons

208 were conducted on melt procedures of an ice sample from the ice tank. Measurements  
209 of ChlF were performed on three treatments of ice samples; (1) intact ice, (2) slushy  
210 melted ice suspended in filtered seawater (ice: seawater ratio=1: 1), (3) slowly (24 h)  
211 and directly melted samples. The blank calibration for  $F_o$  was conducted with filtered  
212 seawater as described, however, an empty quartz tube was used for the calibration  
213 because it was impossible to prepare a blank ice sample for the treatment 1. It was thus  
214 assumed that the ice samples for the treatment had a high enough biomass without  $F_o$   
215 calibration. All samples were stored or melted in the dark for 30 min for the treatments  
216 1 and 2, whereas the other samples (i.e. the treatment 3) were kept at 2.5 °C during the  
217 overnight melting. The FRRf was used for the ice samples from the ice tank as  
218 described above.

219

#### 220 *Cell abundance of ice algae*

221 Triplicated microscopic samples were fixed with neutralized formaldehyde solution  
222 (final concentration 2%). Cell abundance of *F. cylindrus* was determined with an  
223 inverted microscope (Axiovert 25, Zeiss) and a Sedwick-Rafter counting chamber  
224 (Pysen-SGI Lmd.). At least 500 cells were enumerated to determine cell abundance  
225 (LeGresley and McDermott 2010). Growth rate was calculated following Wood et al.

226 (2005):

228 
$$\mu = \frac{\ln(N_t/N_0)}{t - t_0}$$

227

229 *Pigment composition*

230 Pigment concentrations were determined to quantify chlorophylls, photosynthetic and  
231 photoprotective carotenoids, and chlorophyll derivatives with a Ultra-High Performance  
232 Liquid Chromatography (UHPLC) (Suzuki et al. 2015). On each sampling day,  
233 triplicated ice or seawater samples were filtered onto 25 mm GF/F filters (Whatman)  
234 using gentle vacuum (<0.013MPa) via a 25 mm polypropylene in-line filter holder  
235 (Swinnex, Merck). Rintala et al. (2014) confirmed that fast and direct melting was a  
236 reliable method for pigment analysis in ice algae. The filter was flash frozen in liquid  
237 nitrogen and stored in a deep freezer (−80 °C). After thawing, the filter was blotted dry  
238 with a filter paper, and the pigments were extracted using the *N, N*-dimethylformamide  
239 (DMF) bead-beating method (Suzuki et al. 2015). The extracted pigments were  
240 suspended in DMF and then injected into an UHPLC for pigment determination. The  
241 ratio of diadinoxanthin (DD) and diatoxanthin (DT) was calculated to assess the  
242 xanthophyll epoxidation-de-epoxidation cycle and photoprotective strategies of algae  
243 (Katayama et al. 2017), assessed as a de-epoxidation state (DES; DT/(DD+DT)). Total

244 chl *a* (Tchl *a*: sum of chl *a*, chlorophyllide *a*, chl *a*-allomer, and chl *a*-epimer)  
245 concentrations were calculated as an indicator of algal biomass. Contributions of  
246 chlorophyllide (chllide *a*) *a* to Tchl *a* were also calculated as an index of the breakdown  
247 of chl *a*. Following Schuback et al. (2016) and Yan et al. (2019), ratios of  
248 photoprotective carotenoids (PPC: DD, DT, and  $\beta,\beta$ -carotene) to photosynthetic  
249 carotenoids (PSC: only fucoxanthin here) in diatoms and the xanthophyll pool size  
250  $((DD+DT)/Tchl\ a)$  were calculated to quantify photoprotective potentials of the diatom  
251 *F. cylindrus*.

252

253 *Gene expression of photosynthesis-related genes; psbA and rbcL*

254 To investigate the mechanisms of freezing and melting stress on cells of *F. cylindrus*  
255 in water and in the ice, gene expression of the photosynthesis-related genes, *psbA* and  
256 *rbcL*, was measured. To stabilize the RNA, 250  $\mu$ L of RNAlater (Sigma) was  
257 immediately added to the ice core after collection. Triplicated melted ice and seawater  
258 samples were filtered onto two 25 mm, 2  $\mu$ m polycarbonate Isopore membrane filters  
259 (Millipore) with gentle vacuum ( $<0.013$ MPa) passing through a 25 mm polypropylene  
260 in-line filter holder (Swinnex, Merck) for DNA and RNA samples. The DNA samples  
261 were placed in a cryotube and flash frozen in liquid nitrogen and stored at  $-80$  °C. RNA

262 samples were suspended in 600  $\mu$ L RLT buffer (Qiagen) in a cryotube, to which 10  $\mu$ L  
263 of  $\beta$ -mercaptoethanol (Sigma-Aldrich) was added. The RNA sample then was flash  
264 frozen in liquid nitrogen prior to storage at  $-80$   $^{\circ}$ C until further analysis. DNA and RNA  
265 were extracted following Endo et al. (2013) and Endo et al. (2015), respectively. The  
266 extracted RNA was reverse-transcribed to complementary DNA (cDNA) with the  
267 PrimeScript<sup>TM</sup> RT Master Mix (RR036, Takara) reagent according to the  
268 manufacturer's specification. DNA and cDNA copy numbers of the *psbA* and *rbcL*  
269 genes were quantified by quantitative PCR (qPCR). The primer sets and PCR conditions  
270 used in this study are shown in Table S1 in the Supporting Information. Gene  
271 expression was defined as the ratio of copy numbers of cDNA to DNA.

272

### 273 *Statistical analysis*

274 Statistical analyses were conducted using the SigmaPlot software program ver. 11.0  
275 (SystStat Software, Inc.). One-way ANOVA with Tukey's test was performed on the  
276 individual sampling days in each light treatment to identify variations in ChlF  
277 parameters, pigment concentrations and gene expression. The differences in each  
278 parameter were considered significant when  $p < 0.05$ . Two-way ANOVA with Tukey's

279 tests was performed on the individual sampling days and light treatment to identify the  
280 differences in ChlF and pigment data to assess the effects of differences in  
281 photosynthetic ability and pigment composition between light treatments. Data was  
282 transformed for normalization prior to the ANOVA tests with the R statistical software  
283 using the R package MASS. Normality and variance of the data were checked by  
284 performing Shapiro-Wilk's test and Levene's test using the SigmaPlot software  
285 program after the data transformation, respectively.

286

## 287 RESULTS

### 288 *Ice physics and ice algal growth*

289 During the experiments, ice thickness remained stable at 5.5 cm with little basal  
290 melting or sublimation. Temperature within the ice increased with depth (ice surface:  
291  $-22.5\text{ }^{\circ}\text{C}$ , ice-water interface:  $-2.2\text{ }^{\circ}\text{C}$ ) (Fig. 2) and the underlying seawater was stable  
292 at ca.  $-1.8\text{ }^{\circ}\text{C}$  throughout the incubations. Brine salinity decreased with depth from  
293  $293.7 \pm 0.0$  to  $39.4 \pm 0.5$ , whereas the brine fraction increased ( $3.7 \pm 0.0\%$  to  $34 \pm 0\%$ ,  
294 assuming no gas bubbles were present). Nutrient concentrations did not significantly  
295 change during the incubations (data not shown). The ice formation concentrated *F.*  
296 *cylindrus* cells in the ice (HL:  $8883 \pm 224\text{ cells mL}^{-1}$ ; LL:  $8600 \pm 573\text{ cells mL}^{-1}$ )

297 compared with under-ice seawater ( $3551 \pm 95$  cells  $\text{mL}^{-1}$ ; LL:  $3639 \pm 135$  cells  $\text{mL}^{-1}$ ).  
298 Cells of *F. cylindrus* were thus successfully incorporated into the ice matrix where slow  
299 but positive growth in both treatments was observed ( $0.020 \pm 0.001$  and  $0.020 \pm 0.002$   
300 under HL and LL, respectively); there was no significant difference in growth rate  
301 between the treatments ( $t=0.00$ ,  $p>0.05$ , Welch's *t*-test).

302

303 *Variable chl a fluorescence*

304 *Dark values ( $F_v/F_m$  and  $\sigma_{PSII}$ )*

305 At the beginning of the incubations (day -05), initial  $F_v/F_m$  of *F. cylindrus* showed  
306 comparable and relatively high values in both high light (HL:  $0.47 \pm 0.05$ ) and low light  
307 (LL:  $0.45 \pm 0.06$ ) conditions ( $t=0.63$ ,  $p>0.05$ , Welch's *t*-test) (Fig. 3A, B). Upon  
308 freezing in (day 00),  $F_v/F_m$  decreased significantly to 0.2–0.3 in both HL and LL (HL:  
309  $F_{(7,40)}=143.27$ ,  $q=31.26$ ,  $p<0.001$ ; LL;  $F_{(7,40)}= 501.93$   $q=35.77$ ,  $p<0.001$ , one-way  
310 ANOVA, Tukey's test) (Fig. 3A, B), while  $\sigma_{PSII}$  did not change (HL:  $F_{(7,40)}=10.59$ ,  
311  $q=2.01$ ,  $p>0.05$ ; LL:  $F_{(7,40)}= 12.97$ ,  $q=3.65$ ,  $p>0.05$ , one-way ANOVA) (Fig. 3C, D).  
312 Once incorporated into the ice matrix the  $F_v/F_m$  of *F. cylindrus* cells remained stable  
313 from day 00 to day 20 regardless of the light availability (HL:  $0.20 \pm 0.03$ ; LL:  $0.16 \pm$   
314  $0.05$ ,  $t=1.68$ ,  $p>0.05$ , Welch's *t*-test), until initiation of the melt cycle. The lowest  $F_v/F_m$

315 was observed on day 15 in both HL and LL (HL:  $0.18 \pm 0.02$ ; LL:  $0.09 \pm 0.02$ ) (Fig.  
316 3A, B). The  $\sigma_{\text{PSII}}$  values at both light levels were relatively stable throughout the  
317 incubations with slight decreases with time (Fig. 3C, D). Once the ice had melted,  
318  $F_v/F_m$  values seemed to be recovered from the values at day 20 in LL (HL:  $0.18 \pm 0.02$ ;  
319 LL:  $0.19 \pm 0.02$ ) to almost equivalent levels on day -05 (see above), respectively. There  
320 were, however, significant differences in  $F_v/F_m$  values between day -05 and melt  
321 samples both in HL and LL (HL:  $q=35.57, p<0.001$ ;  $q=35.77, p<0.001$ , one-way  
322 ANOVA, Tukey's test) ( $39 \pm 1\%$  lower and  $15 \pm 1\%$  higher, respectively) (Fig. 3A, B).  
323 The responses of  $\sigma_{\text{PSII}}$  differed to  $F_v/F_m$ , which was significantly different on day -05,  
324 but similar to  $\sigma_{\text{PSII}}$  values on day 20 regardless of the light availability (HL:  $q=1.07,$   
325  $p>0.05$ ; LL:  $q=1.08, p>0.05$ , one-way ANOVA) (Fig. 3C, D). Immediately after light  
326 exposing the melted samples at  $800 \mu\text{mol photons m}^{-2} \text{s}^{-1}$ ,  $F_v/F_m$  significantly  
327 decreased in both light treatments (HL:  $q=13.09, p<0.001$ ; LL:  $q=53.11, p<0.001$ , one-  
328 way ANOVA, Tukey's test) ( $39 \pm 3\%$  and  $29 \pm 2\%$  for HL and LL treatments,  
329 respectively). Despite the large decreases in  $F_v/F_m$ ,  $\sigma_{\text{PSII}}$  showed minimal variation.

330

331 *Non-photochemical quenching (NPQ<sub>NSV</sub>' )*

332 Values of non-photochemical quenching (NPQ<sub>NSV</sub>' ) in both light treatments were low

333 on day -05 prior to freezing in. Upon ice incorporation,  $\text{NPQ}_{\text{NSV}}$ ' significantly  
334 increased in both HL and LL treatments (HL:  $F_{(7,40)} = 52.55$ ,  $q=44.54$ ,  $p<0.001$ ; LL:  
335  $F_{(7,40)} = 149.81$ ,  $q=10.10$ ,  $p<0.001$ , one-way ANOVA, Tukey's test) (Fig. 4).  $\text{NPQ}_{\text{NSV}}$ '  
336 in HL plateaued immediately after ice formation (i.e., day 00), while  $\text{NPQ}_{\text{NSV}}$ ' in LL  
337 was observed to gradually increase and reach a maximum on day 05 (Fig. 4). Post ice  
338 melt,  $\text{NPQ}_{\text{NSV}}$ ' in the LL tank decreased to the identical levels as those observed on day  
339 -05 ( $q=1.36$ ,  $p>0.05$ , one-way ANOVA), whereas the HL treatment showed a  
340 significant increase in  $\text{NPQ}_{\text{NSV}}$ ' ( $q=6.676$ ,  $p<0.001$ , one-way ANOVA, Tukey's test).  
341 The light exposure after the melting event significantly enhanced  $\text{NPQ}_{\text{NSV}}$ ' (almost  
342 doubled) in both HL and LL treatments (HL:  $q=11.39$ ,  $p<0.001$ ; LL:  $q=5.22$ ,  $p=0.012$ ,  
343 one-way ANOVA) (Fig. 4).

344

#### 345 *Photosynthesis-irradiance ( $\text{ETR}_{\text{RCII-E}}$ ) curve*

346 The initial slopes of  $\text{ETR}_{\text{RCII-E}}$  curve,  $\alpha$  (regarded as light utilization efficiency),  
347 dropped significantly when the algae were frozen into the ice (HL:  $F_{(7,40)} = 8.20$ ,  $q=6.84$ ,  
348  $p<0.001$ ; LL:  $F_{(7,40)} = 11.27$ ,  $q=8.24$ ,  $p<0.001$ , one-way ANOVA, Tukey's test) but did  
349 not significantly differ thereafter in HL treatment ( $p>0.05$ , one-way ANOVA) (Fig. 5A,  
350 B). A similar trend was observed in the LL treatment, although  $\alpha$  increased significantly

351 towards the end of the incubation ( $p < 0.05$ , one-way ANOVA, Tukey's test). After the  
352 ice melted,  $\alpha$  values did not significantly change in HL ( $q = 0.97$ ,  $p > 0.05$ , one-way  
353 ANOVA), while, in LL,  $\alpha$  returned the initial levels at day -05. Maximum electron  
354 transport rates ( $ETR_{\max}$ ) in both treatments significantly decreased upon freezing in  
355 (HL:  $F_{(7,40)} = 7.63$ ,  $q = 11.85$ ,  $p < 0.001$ ; LL:  $F_{(7,40)} = 86.30$ ,  $q = 18.52$ ,  $p < 0.001$ , one-way  
356 ANOVA, Tukey's test) (from  $281 \pm 37$  and  $300 \pm 67$  to  $111 \pm 53$  and  $38 \pm 13$  in HL and  
357 LL treatments, respectively). Upon melting out,  $ETR_{\max}$  in LL returned ( $335 \pm 57$ ) to  
358 the initial levels at day -05 ( $q = 2.40$ ,  $p > 0.05$ , one-way ANOVA), whereas, in HL,  
359  $ETR_{\max}$  was not recovered ( $q = 14.41$ ,  $p < 0.001$ , one-way ANOVA, Tukey's test) (Fig.  
360 5C, D). Light saturation indices,  $E_k$ , gradually decreased during the course of the  
361 incubation experiments without any conspicuous variation during the frozen period  
362 (Fig. 5E, F). The HL treatment showed higher  $E_k$  throughout the frozen period from day  
363 05 to day 20 compared to LL ( $F_{(1,40)} = 9.02$ ,  $p = 0.004$ , two-way ANOVA, Tukey's test).  
364 When melted out,  $E_k$  values returned to the initial levels on day -05 in both treatments  
365 although the LL treatment show a higher  $E_k$  (HL:  $F_{(7,40)} = 7.63$ ,  $q = 0.63$ ,  $p > 0.05$ ; LL:  
366  $F_{(7,40)} = 66.51$ ,  $q = 12.30$ ,  $p < 0.001$ , one-way ANOVA, Tukey's test). On the other hand,  
367  $E_k$  significantly decreased in both HL and LL treatments (HL:  $q = 8.20$ ,  $p < 0.001$ ; LL:  
368  $q = 7.91$ ,  $p < 0.001$ , one-way ANOVA, Tukey's test) (Fig. 5E, F).

369

370 *Validation experiments for sample melt procedures*

371 Variable ChlF parameters varied among the different melt procedures of the ice sample  
372 (Fig. S2 in the Supporting Information). When the intact crushed ice sample was packed  
373 directly into a quartz tube,  $F_v/F_m$  values were lower, followed by that of the slushy  
374 melted sample. These values were almost the same and did not show any significant  
375 difference ( $F_{(2,7)}=10.76$ ,  $q=2.90$ ,  $p>0.05$ , one-way ANOVA), whereas the slow-direct  
376 melt sample showed a significantly higher value compared to its counterparts ( $q=4.94$ ,  
377  $p=0.024$ , one-way ANOVA, Tukey's test). Unlike  $F_v/F_m$  values,  $\sigma_{PSII}$  varied little  
378 regardless of the melt methods and did not show any significant enhancement or  
379 suppression ( $F_{(2,7)}=3.31$ ,  $p>0.05$ , one-way ANOVA) (Fig. S2 in the Supporting  
380 Information).

381

382 *Pigment composition*

383 Initial Tchl *a* concentrations were at the same level between incubations at day-05  
384 ( $F_{(1,31)}=2.29$ ,  $p>0.05$ , Two-way ANOVA) (Fig. 6A, B). After *F. cylindrus* cells were  
385 incorporated into the ice, ice algae in the HL treatment maintained stable Tchl *a*  
386 biomass ( $F_{(7,16)}=2.27$ ,  $q=0.09$ ,  $p>0.05$ , one-way ANOVA) although Tchl *a* in the LL

387 treatment showed a gradual increase. Contributions of chl *a* to Tchl *a* were slightly  
388 higher in the HL treatment than in the LL tank throughout the incubations  
389 ( $F_{(1,31)}=59.96$ ,  $p<0.001$ , Two-way ANOVA, Tukey's test; 48.0–62.5% and 34.0–54.9%,  
390 respectively) (Fig. 6A, B). The cellular DD-DT pool size in both the HL and LL  
391 treatments at the beginning of the incubations was comparable ( $F_{(1,31)}=73.27$ ,  $q=1.76$ ,  
392  $p>0.05$ , Two-way ANOVA), whereas, during the frozen period the cellular pool size  
393 grew faster was significantly larger in the HL ice tank than those in the LL tank  
394 ( $F_{(7,16)}=73.27$ ,  $q=12.11$ ,  $p<0.001$ , Two-way ANOVA, Tukey's test; 17.3–25.3% and  
395 8.8–14.7% to Tchl *a*, respectively) (Fig. 6C, D). During the frozen period from day 05  
396 to day 20, DES was also higher in the HL ice tank (0.293–0.552) compared to the LL  
397 ice tank (0.107–0.231) ( $F_{(1,31)}=35.65$ ,  $p=0.027$ , Two-way ANOVA, Tukey's test) (Fig.  
398 6C, D). Light exposure enhanced the DES in both treatments (4.20- and 5.23-fold  
399 increases in the HL and LL ice tank, respectively). Higher PPC/PSC ratios were present  
400 in the HL ice tank than in LL throughout the incubations ( $F_{(1,31)}=69.22$ ,  $p<0.001$ , Two-  
401 way ANOVA, Tukey's test) (Fig. 6E, F). The PPC/PSC ratios showed little variation  
402 before and after light exposure in both light treatments (HL:  $F_{(7,16)}=3.82$ ,  $q=0.04$ ,  
403  $p>0.05$ ; LL:  $F_{(7,16)}=3.86$ ,  $q=0.85$ ,  $p>0.05$ , one-way ANOVA).

404

405 *Gene expression of photosynthesis-related genes*

406 *rbcL*

407 Prior to incubation there was no significant difference in the expression of the *rbcL*  
408 gene in either HL or LL ( $t=0.33$ ,  $p>0.05$ , Welch's *t*-test) (Fig. 7A, B). Transcriptional  
409 activity of the *rbcL* gene was highly upregulated when algae were frozen into the ice  
410 (HL:  $F_{(7,16)}=7.65$ ,  $q=5.30$ ,  $p=0.03$ ; LL:  $F_{(7,16)}=7.39$ ,  $q=6.89$ ,  $p=0.003$ , one-way  
411 ANOVA, Tukey's test) in both HL and LL (Fig. 7A, B). After day 05 and day 10, gene  
412 expression of the *rbcL* gene decreased significantly in the HL and LL treatments (HL:  
413  $q=7.290$ ,  $p=0.002$ ; LL:  $q=6.79$   $p=0.040$ , one-way ANOVA, Tukey's test), respectively  
414 (Fig. 7A, B). This low level was sustained during the frozen period. Comparing the  
415 results of melt and light periods, the *rbcL* gene expression did not show any  
416 conspicuous change in either treatment (HL:  $q=2.173$ ,  $p>0.05$ ; LL:  $q=0.31$ ,  $p>0.05$ ,  
417 one-way ANOVA).

418

419 *psbA*

420 Unlike the *rbcL* gene, the expression of the *psbA* gene differed with respect to light  
421 availability (Fig. 7C, D). The initial value in the HL treatment was ~2-fold higher than  
422 that in LL. In HL, transcription of the *psbA* gene was highly upregulated during freezing

423 ( $F_{(7,16)}=19.90$ ,  $q=10.28$ ,  $p<0.001$ , one-way ANOVA, Tukey's test); which was similar  
424 to the *rbcL* gene. In LL, upregulation of *psbA* was not evident ( $F_{(7,16)}=2.02$ ,  $p>0.05$ ,  
425 one-way ANOVA). Expression of *psbA* in HL showed a similar trend to the *rbcL* gene,  
426 whereas, under LL, the *psbA* gene expression did not change throughout the experiment  
427 (Fig. 7C, D).

428

## 429 DISCUSSION

### 430 *Ice tank incubation*

431 We here, for the first time, successfully demonstrated the use of a purpose designed ice  
432 tank to study the photophysiology of ice algae for a prolonged period (i.e. 20 days)  
433 under environmentally relevant conditions. When ice formed, cooling of the water body  
434 from the surface in the ice tank, in a  $-20$  °C freezer, realistically mimicked *in situ* ice  
435 formation events in wintertime, with cells of *F. cylindrus* successfully incorporated into  
436 the ice. The temperature profile of the artificial sea ice indicates that the ice properties  
437 simulated winter ice environments, inferred from a sharp decrease in temperature with  
438 depth (Fig. 2) (Petrich and Eicken 2017). It suggests that the ice tank was well suited to  
439 investigate survival strategies of ice algae under chronic multiple stress in wintertime.

440 The identical initial  $F_v/F_m$  values at day-05 (Fig. 3A, B) indicate that the two discrete  
441 ice tank runs (i.e. HL and LL treatments) started with the similar physiological states of  
442 *F. cylindrus*.

443

#### 444 *Freezing event*

445 The freezing events in the ice tank experiments reported herein suppressed  
446 photochemical quantum efficiency of PSII (Fig. 3A, B). Drawdowns in  $F_v/F_m$  were also  
447 observed in the previous ice tank study using *Phaeocystis antarctica* (Kennedy et al.  
448 2012) during ice formation. This suppression has also been noted in natural sea ice,  
449 inferred from lower  $F_v/F_m$  of ice algae than pelagic phytoplankton (McMinn et al.  
450 2008, Yamamoto et al. 2014).

451 A significant amount of chl *a* breakdown products has been reported in ice algae of  
452 both landfast and pack-ice in the Arctic and Antarctic (e.g., Horner 1985, Alou-Font et  
453 al. 2013). One might interpret the here observed increase in chl *a* (Fig. 6A, B) as  
454 inactivation of PSII reaction centres. Chl *a*, lacking the phytol chain, has a less  
455 pigment aggregation potential (Fiedor et al. 2003), leading to reduced coupling of  
456 excitons (inefficient energy transfer between pigments) (Rosenbach-Belkin et al. 1991).

457 However, the stable amount of chl *a* during the freezing events (Fig. 6A, B)  
458 indicates that the existence of chl *a* had only a minor effect on the drawdown in  
459  $F_v/F_m$ . Also, not all inactive pigments (i.e. chl *a*) are involved in reaction centres  
460 but function as photosynthetic antennae pigments.

461 Suggett et al. (2009) demonstrated that chronic stress decreases  $F_v/F_m$  with a  
462 concomitant enhancement of  $\sigma_{PSII}$  because of the absorbed light energy being funnelled  
463 to fewer active PSII reaction centres if some reaction centres are damaged/inactive  
464 (Suggett et al. 2009, 2011, Falkowski and Raven 2013). In this study, however, little  
465 variation in  $\sigma_{PSII}$  was observed during the freezing event (Fig. 3C, D). This suggests that  
466 photoinactivation could not be significant during ice formation.

467 Freezing stress, combined with low temperatures and high brine salinity, could be the  
468 main cause of the reduction in the photochemistry of PSII and the capacity of electron  
469 sinks (Ensminger et al. 2006, Ralph et al. 2007). Low temperatures reduce membrane  
470 viscosity, which suppresses photochemical reactions in the electron transport chain  
471 (Morgan-Kiss et al. 2006). At the same time, high brine salinity might suppress the  
472 reduction capability of electron donors around PSII (i.e., the first quinone electron  
473 acceptor  $Q_A$  and the plastoquinone (PQ) pool; Ralph et al. 2007). Indeed, the here

474 observed high brine salinity (55 on average and >80 in the upper part of the ice) was  
475 high enough to suppress the downstream components of PSII (Ralph et al. 2007). This  
476 combined stress of low temperature and high salinity has been found to stagnate  
477 electron transfer along the electron transport chain down to ferredoxin and cause  
478 “electron clogging” (e.g., Lazár et al. 2005). This “electron clogging” consequently can  
479 lead to (a) the low  $F_v/F_m$  (e.g., Schwarz et al. 2017), (b) overreduction of the PQ pool  
480 (Maxwell et al. 1995, Allen and Nilson 1997, Pfannschmidt 2003) and (c) an imbalance  
481 of the photochemical electron transport (“photostasis”; Öquist and Huner 2003). We  
482 interpret the here observed increase in  $NPQ_{NSV}$  (Fig. 4) as a measure for alleviating  
483 excess excitation pressure (e.g. Caron et al. 1987, Ting and Owens 1993, Goss and  
484 Jakob 2010).

485 The HL treatment exhibited a larger DD-DT pool and higher PPC/PSC compared with  
486 the LL counterpart (Fig. 6C, D, E, F). These light responses can be interpreted as up-  
487 front protection to mitigate the production of reactive oxygen species under high light  
488 (McMinn and Hegseth 2004, Katayama and Taguchi 2013, Kuczynska et al. 2015). This  
489 notion is supported by field observations of (Kropuenske et al. 2009, Schuback et al.  
490 2016, Galindo et al. 2017) and emphasized light-photoprotection relationships (Lavaud  
491 et al. 2002, Domingues et al. 2012).

492 Photosynthetic performance, assessed with  $ETR_{RCII}-E$  curves, showed rapid  
493 photoacclimation responses during freezing; a greater decrease in  $ETR_{max}$  than that of  $\alpha$   
494 led to apparent dark acclimation with a lower  $E_k$  after freezing (Fig. 5). However, the  
495 concomitant decrease of  $\alpha$  does not coincide with classical shade photoacclimatisation  
496 strategies (i.e. higher  $\alpha$  and lower  $E_k$  under lower light would be expected; MacIntyre et  
497 al. 2002). The decrease in  $\alpha$  suggests a decrease in  $n_{PSII}$ , the active fraction of PSII to  
498 chl *a* (e.g. Falkowski and Raven 2013). Values of  $\alpha$  are represented as a product of  $\sigma_{PSII}$   
499 and  $n_{PSII}$ ; however,  $\sigma_{PSII}$  values were stable during the freezing event, suggesting  
500 photoinactivation of RCII (i.e., lowered  $n_{PSII}$ ). It is thus suggested that both the  
501 combination of direct photoinactivation and electron clogging deactivated the  
502 photochemical reactions at RCII. The freezing event, therefore, suppressed RCII  
503 photochemistry both directly and indirectly.

504 The strong upregulation of expression of the *psbA* gene in the HL treatment  
505 accelerated repair of damaged PSII under overexcitation pressure in the HL condition  
506 and vice versa (Fig. 7C, D) (Petrou et al. 2010, Galindo et al. 2017). The significant  
507 upregulation of the *rbcL* gene (Fig. 7A, B) could be evidence of a cold acclimation  
508 strategy to increase cellular RuBisCO and compensate for the low catalytic activity of  
509 the temperature-sensitive enzyme by increasing its concentration (Devos et al. 1998,

510 Lyon and Mock 2014, Young et al. 2015). However, Mock and Hoch (2005) reported  
511 downregulation of *rbcL* transcription in *F. cylindrus* under low temperatures.  
512  
513 *During the frozen period*  
514 ChlF parameters remained relatively stable during the frozen period and little variation  
515 in  $F_v/F_m$ ,  $\sigma_{PSII}$ , and NPQ<sub>NSV</sub> values were observed within the ice (Figs. 3 and 4),  
516 indicating that sea ice is a stable platform for algal photosynthesis (Maccario et al.  
517 2015, Arrigo 2017). The comparable levels of  $F_v/F_m$  and  $\sigma_{PSII}$  in both ice tanks suggest  
518 that the *F. cylindrus* cells sustained or optimized their photosynthesis within the ice  
519 regardless of light availability (Fig. 3). This physiological acclimation to ice  
520 environments may play a key role in the successful survival and proliferation of ice  
521 algae within and at the bottom of sea ice (Kropuenske et al. 2010, Lacour et al. 2018).  
522 McMinn and Hegseth (2004) suggested that ice diatoms can grow out in sea ice if  
523  $F_v/F_m$  is  $>0.125$ . In this study, the observed  $F_v/F_m$  values during the frozen period were  
524 high enough to actively grow in the ice. Indeed, this study, for the first time, reported  
525 positive growth in the ice tank. Although the growth rates in both treatments ( $\sim 0.02\text{ d}^{-1}$ )  
526 were lower than other reported values from culture experiments (e.g., Mock and Hoch  
527 2008, Kropuenske et al. 2010). Interestingly, the growth rates in both the HL and LL

528 treatments were comparable regardless of the under-ice light intensities. This indicates  
529 that light availability was not a limiting factor for algal growth in the artificial sea ice.  
530 Evidently, photosynthetic and photoprotective abilities between the HL and LL ice  
531 tanks were comparable during the frozen periods, as inferred from the identical levels of  
532  $F_v/F_m$  and  $NPQ_{NSV}$  (Fig. 3A, B; Fig. 4). As discussed above, the electron clogging  
533 caused by multiple co-stressors could be the major determinant of algal growth. The  
534 low temperature lowered the enzymatic activity of RuBisCO (Young et al. 2015), which  
535 could be another possible cause of the identical growth rates observed in both HL and  
536 LL treatments. The gradual increase in light utilization index  $\alpha$  in the LL ice tank (Fig.  
537 5A, B) was consistent with the classical concept of photoacclimation (MacIntyre et al.  
538 2002). As noted above,  $\sigma_{PSII}$  was stable in the LL treatment (Fig. 3C, D). Cells under  
539 LL may increase the proportion of active RCII relative to pigmentation (chl *a*) in order  
540 to enhance light capture during freezing in (Fig. 5E, F). Only algae in the LL ice tank  
541 showed a gradual increase in Tchl *a* concentration, in spite of the same algal growth rate  
542 in both HL and LL treatments; this could be further evidence of dark acclimation (e.g.,  
543 Falkowski and Owens 1980). The smaller PPC/PSC in the LL ice tank also supports this  
544 suggestion by indicating preferential synthesis of photosynthetic chlorophylls and  
545 carotenoids rather than PPC (Fig. 6E, F). Cells in the HL treatment strengthened their

546 photoprotective capability, reflected in higher values of PPC/PSC and DES compared to  
547 cells in LL (Fig. 6C, D, E, F) (Kropuenske et al. 2009, 2010). However, both HL and  
548 LL treatments showed increased their DD-DT pool and DES, suggesting again a highly  
549 reduced PQ pool due to the electron clogging (i.e., the development of  $\Delta pH$ ) (Leptit et  
550 al. 2010, 2013). Interestingly,  $NPQ_{NSV}$ ' levels were comparable between the light  
551 treatments regardless of the difference in DES (Figs. 4 and 5C, D). Nymark et al. (2013)  
552 suggested that low-light acclimated cells have more *LHCX* proteins, which enlarges  
553 their NPQ capacity (Bailleul et al. 2010). Interestingly, the transcriptional activity of the  
554 *rbcL* gene greatly decreased after the sharp increase on day 00 (onset of freezing),  
555 suggesting that cells had used the high abundance of RuBisCO (or its mRNA) that was  
556 synthesized during the freezing event (Fig. 7A, B). The constant but lower expression of  
557 *psbA* could keep the repair of PSII to a 'business as usual' rate (Fig. 7C, D), whereas the  
558 downregulation of the gene after initial significant upregulation in the HL treatment  
559 might be caused to alleviate the photochemical imbalance in the electron transport chain  
560 due to the upregulation when shocked by freezing stress (e.g. changes in PSII to PSI  
561 ratio).

562

563 *Light exposure after ice melt*

564 Light exposure to released algal cells in spring time suppressed photosynthetic  
565 activities. Exposure to irradiance following melting decreased  $F_v/F_m$  due to the high  
566 excitation pressure (Fig. 3A, B), despite ice melt before light exposure increasing  
567 photochemical activity. The increase in  $F_v/F_m$  after ice melt was consistent with results  
568 of the validation experiments (Fig. S2 in the Supporting Information). The degree of  
569 drawdown in  $F_v/F_m$  was comparable regardless of the incubation light intensity after  
570 light exposure (Fig. 3A, B).  $NPQ_{NSV}$  was downregulated when the ice melted but was  
571 enhanced after light exposure (Fig. 4). This reverse response to light exposure between  
572  $F_v/F_m$  and  $NPQ_{NSV}$  might be evidence for fast activation of photoprotection (Figs. 3A,  
573 B and 4) especially in the HL treatment with the higher DES (Fig. 6C, D). Damage of  
574 PSII, however, was likely because of the considerable increase in the ratio of chl *a*  
575 to Tchl *a* after light exposure in both ice tanks (Fig. 6A, B). One might suspect that the  
576 melting process prior to sample filtration caused the significant breakdown of chl *a* with  
577 activation of chlorophyllase (Jeffery and Hallegraeff 1987); however, a stable level of  
578 chl *a* to Tchl *a* observed throughout the incubation period even from day -05 before  
579 ice formation (Fig. 5A, B) suggests the melting process (osmotic stress) could not be  
580 responsible for the high concentrations of chl *a* and other degraded pigments.  
581 However, the significant difference in chl *a* contributions between HL and LL

582 throughout the incubations might relate to the breakdown of chl *a* because high light to  
583 *F. cylindrus* leads a high qI (non-photochemical quenching by photoinactivation)  
584 (Kropuenske et al. 2009). After ice melt, PPC/PSC decreased while  $F_v/F_m$  increased  
585 (Figs. 3A, B and 6E, F). This suggests a re-optimization of photosynthetic performance  
586 to a water environment after release from freezing stress. Light exposure, however,  
587 activated the DD-DT xanthophyll cycle (i.e., de-epoxidation) (Fig. 6C, D) (Petrou et al.  
588 2010), although the size of the DD-DT pool was little changed (Fig. 6C, D). Activation  
589 of the DD-DT cycle is the fastest photoprotective strategy and occurs at a scale of  
590 seconds to minutes (Goss and Jakob 2010), whereas the size of the pool actually  
591 changes much slower. Interestingly, NPQ<sub>NSV</sub>' in the HL treatment was much higher  
592 than that of the LL treatment with differences in their DD-DT pool size (Figs. 4 and 6C,  
593 D), suggesting that pigmentation and light history were largely responsible for their  
594 potential photoprotective ability (Szechyńska- Hebda et al. 2010, Galindo et al. 2017). It  
595 seems to be unusual that  $E_k$  values significantly decreased (i.e. dark acclimation) upon  
596 light exposure, contrary to the expected response from high-light acclimation (Fig. 5E,  
597 F). Transcriptional activity of the *psbA* gene was stable in both treatments after light  
598 exposure (Fig. 7C, D). It is suggested that algal cells did not immediately start to  
599 synthesize mRNA for repair of the damaged RCII, possibly because post-transcriptional

600 regulation is significant for D1 protein synthesis (Malnoë et al. 1988, Danon and  
601 Mayfield 1991) with a large mRNA pool (Mulo et al. 2012). The dark reaction might  
602 also be independent or to have been slow to respond to the light exposure event because  
603 the gene expression of the *rbcL* gene was invariant before and after light exposure (Fig.  
604 6A, B).

605

## 606 CONCLUSIONS

607 This study demonstrates how the combined effects of ice formation and melting  
608 together with light exposure affect the photophysiology of *F. cylindrus*. This study is  
609 the first attempt to conduct the *ex situ* incubation of the ice algal *F. cylindrus* in  
610 artificial sea ice to quantify the effects of multiple co-stressors in sea ice and to provide  
611 new insights into the fate of ice algae. The ice tank successfully mimicked ice formation  
612 events as experienced in the field (Figs. 1 and 2). This enabled investigation into the  
613 effects of multiple co-stressors on the capacity of *F. cylindrus* to survive this ephemeral  
614 habitat. We successfully observed, for the first time, positive growth of ice algal cells in  
615 artificial sea ice. Ice formation events suppressed the photochemical process of RCII,  
616 despite optimal irradiance prior to freezing in (Fig. 3A, B). This was likely a result of  
617 high brine salinity and low temperature, which led to electron clogging in the electron

618 transport chain. Ice algal cells rapidly optimized their photophysiology to the dark  
619 environment within the ice, inferred from decreases in  $E_k$  (Fig. 3 and 5E, F). Light  
620 availability could affect the photoacclimative ability of ice algae, possibly by increasing  
621 active RCII. Further investigation on the connectivity of photosynthetic antennae to  
622 RCII would be needed to address the efficiency of energy transfer to RCII (e.g.,  
623 D'Haene et al. 2015, Yoshida et al. 2018). Although ice melt stimulated algal  
624 photosynthesis, the subsequent light exposure resulted in photoinhibition (Fig. 3A, B)  
625 with significant chl *a* accumulation and NPQ<sub>NSV</sub>' enhancement. However,  
626 photoprotection was rapidly activated. We conclude that the diatom *F. cylindrus*  
627 possesses a high photosynthetic plasticity that contributes to the ecological success of  
628 this species in both pelagic and sea-ice habitats.

629

#### 630 ACKNOWLEDGEMENTS

631 We greatly appreciate the valuable comments provided by the anonymous reviewers.  
632 Thanks to Ms. Akiko Kamimura for her support in pigment analysis. We appreciate  
633 Prof. Philip Boyd for providing his benchtop FRRf. This research was partly supported

634 by Australian Antarctic Science Program (AAS4319) and JSPS Grants-in-Aid for  
635 Scientific Research (JP18H03352, JP17H00775).

636 **LIST OF TABLE**

637 Table 1. Terminology and definition of chlorophyll *a* fluorescence yields obtained from  
638 FRRf fluorometry

639

640 **LIST OF FIGURES**

641 Figure 1. A schematic (A) and a photograph (B) of the 70 L ice tank in a  $-20\text{ }^{\circ}\text{C}$  freezer.

642

643 Figure 2. Vertical profiles of ice temperature ( $T_{\text{ice}}$ ; closed circle), brine salinity ( $S_{\text{br}}$ :  
644 open circle), and the fraction of brine volume ( $V_{\text{br}}$ : closed square) in artificial sea ice in  
645 the ice tank.

646 Error bars indicate 1 standard deviation ( $n=3$ ).

647

648 Figure 3. Maximum photochemical quantum yield of PSII ( $F_v/F_m$ ) (A and B) and  
649 functional absorption cross-section of PSII ( $\sigma_{\text{PSII}}$ ) (C and D) during the ice tank  
650 incubation experiments.

651 Left (A and C) and right (B and D) panels indicate data from the HL and LL treatment,  
652 respectively. Open, closed and shaded bars indicate values of seawater samples before  
653 freezing, ice and seawater samples after melting, respectively. Different letters above  
654 bars in a panel indicate significant differences in values between sampling days with  
655 one-way ANOVA with Tukey's test; there is no significant difference between values if  
656 a given letter is shown in the combination of letters of the counterparts. The D stands  
657 for 'day', while Melt and Light indicate values after melting and light exposure  
658 experiments, respectively. Error bars show 1 standard deviation ( $n \geq 5$ ).

659

660 Figure 4. Non-photochemical quenching based on the normalized Stern-Volmer  
661 quenching coefficient under the actinic light ( $150$  and  $30 \mu\text{mol photons m}^{-2} \text{s}^{-1}$  for HL  
662 and LL, respectively) ( $\text{NPQ}_{\text{NSV}}$ ) during the ice tank incubation experiments. Panels A  
663 and B indicate data from the HL and LL treatments, respectively. Different letters above  
664 bars in a panel indicate significant differences in values between sampling days with  
665 one-way ANOVA with Tukey's test; there is no significant difference between values if  
666 a given letter is shown in the combination of letters of the counterparts. The D stands  
667 for 'day', while Melt and Light indicate values after melting and light exposure  
668 experiments, respectively. Error bars show 1 standard deviation ( $n \geq 5$ ).

669

670 Figure 5. Photosynthesis–irradiance ( $ETR_{RCII}-E$ ) parameters during the ice tank  
671 incubation experiments. Top panels (A and B) show light utilization efficiency under  
672 dim light ( $\alpha$ ) as initial slopes of the  $ETR_{RCII}-E$  curves, middle panels (C and D) indicate  
673 maximum electron transport rate ( $ETR_{max}$ ), and bottom panels (E and F) show light  
674 saturation index ( $E_k$ ). Left (A, C and E) and right (B, D, and F) panels show data from  
675 the HL and LL treatments. Different letters above bars in a panel indicate significant  
676 differences in values between sampling days with one-way ANOVA with Tukey’s test;  
677 there is no significant difference between values if a given letter is shown in the  
678 combination of letters of the counterparts. The D stands for ‘day’, while Melt and Light  
679 indicate values after melting and light exposure experiments, respectively. Error bars  
680 show 1 standard deviation ( $n \geq 5$ ).

681

682 Figure 6. Variations in pigment concentrations during the ice tank incubation  
683 experiments. Top panels (A and B) show total chl *a* concentration (Tchl *a*) [ $\text{mg m}^{-3}$ ]  
684 and contribution of chlorophyllide *a* to Tchl *a*, middle panels (C and D) indicate the size  
685 of DD-DT pool ( $(DD+DT)/Tchl\ a$ ) and de-epoxidation state of xanthophyll pigments

686 (DES; DT/(DD+DT)), and bottom panels (E and F) show ratio of photoprotective  
687 carotenoids (PPC) to the photosynthetic carotenoid (PSC) quantified with UHPLC. Left  
688 (A, C, and E) and right (B, D, and F) show data from the HL and LL treatments,  
689 respectively. The D stands for 'day', while Melt and Light indicate values after melting  
690 and light exposure experiments, respectively. Results of one-way and two-way ANOVA  
691 tests performed on the pigment data were described in the text. Error bars show 1  
692 standard deviation ( $n=3$ ).

693

694 Figure 7. Gene expression [cDNA/DNA] of photosynthesis-related genes. Top (A and  
695 B) and bottom (C and D) panels show gene expression of the *rbcL* and *psbA* genes  
696 during the ice tank incubation experiments. Left (A and C) and right (B and D) show  
697 data from the HL and LL treatments, respectively. Different letters above bars in a panel  
698 indicate significant differences in values between sampling days with one-way ANOVA  
699 with Tukey's test; there is no significant difference between values if a given letter is  
700 shown in the combination of letters of the counterparts. The D stands for 'day', while  
701 Melt and Light indicate values after melting and light exposure experiments,  
702 respectively. Error bars show 1 standard deviation ( $n=3$ ).

703

704 **LIST OF SUPPLEMENTAL MATERIALS**

705 Table S1. Primer sets and PCR conditions of qPCR and qRT-PCR for the *psbA* and

706 *rbcL* genes

707

708 Figure S1. A photo of the ice tank with a light panel.

709 The light panel has a white LED with light diffuser to homogenize the light field over

710 the ice.

711

712 Figure S2. Chlorophyll *a* fluorescence parameters with different melting procedures.

713 (a): Maximum quantum yield of PSII photochemistry ( $F_v/F_m$ ); (b): functional

714 absorption cross-section ( $\sigma_{PSII}$ ), determined with FRR fluorometry.

715 Intact ice: intact ice placed into the cuvette for ChlF measurement; slush; ice sample

716 partially melted in filtered seawater; Direct slow: melted ice sample overnight at 2.5 °C.

717 Different letters indicate significant differences between the given values. Error bars

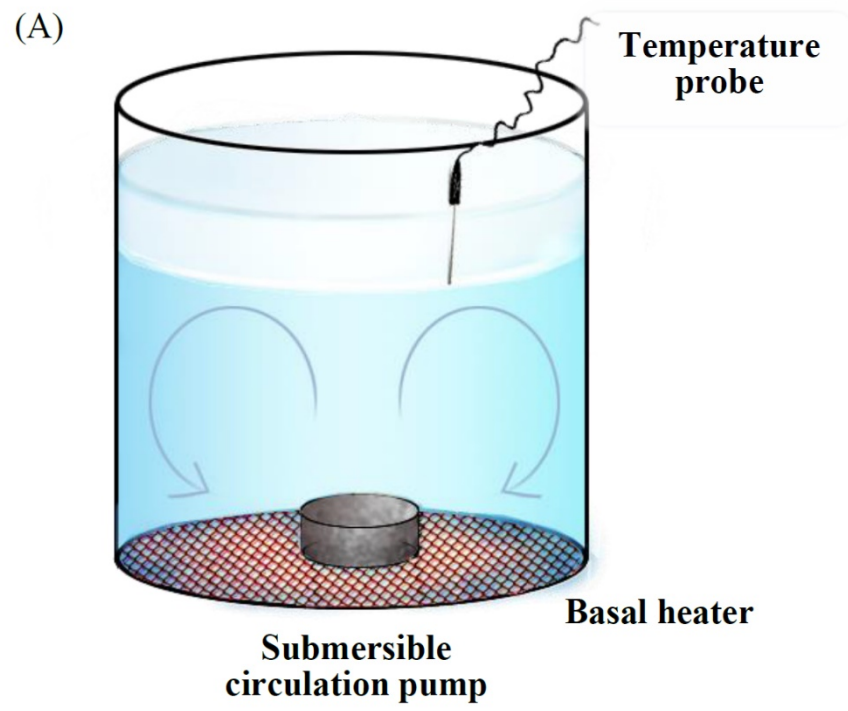
718 indicate 1 standard deviation.  $n=6$ .

Table 1.

Yield and parameter	Unit	Derivation or reference	
<b>Fluorescence yield</b>			
$F$	Fluorescence yield	Unitless	
$F_o$	Minimum fluorescence yield of dark regulated cells	Unitless	
$F_m$	Maximum fluorescence yield of dark regulated cells	Unitless	
$F_v$	Maximum variable fluorescence yield	Unitless	$F_m - F_o$
$F'$	Fluorescence yield under actinic light	Unitless	Oxborough and Baker (1997)
$F_o'$	Minimum fluorescence yield of actinic light-acclimated cells	Unitless	(1997)
$F_m'$	Maximum fluorescence yield of actinic light-acclimated cells	Unitless	
$F_v'$	Variable fluorescence yield under actinic light	Unitless	$F_m' - F_o'$
$F_q'$	Difference in fluorescence yields between $F'$ and $F_m'$	Unitless	$F_m' - F'$
<b>Fluorescence parameters in the dark</b>			
$\sigma_{PSII}$	Functional absorption cross-section of PSII in the dark	$\text{nm}^2 \text{RCII}^{-1}$	Kolber et al. (1998)
$F_v/F_m$	Maximum quantum yield of PSII photochemistry	Unitless	$(F_m - F_o)/F_m$
$\tau$	Time constant for $Q_A$ reoxidation	ms	Kolber et al. (1998)
<b>Fluorescence parameters under actinic light</b>			
$F_q'/F_m'$	Effective photochemical efficiency of PSII under actinic light	Unitless	$(F_m' - F')/F_m'$
$NPQ_{NSV}'$	Non-photochemical quenching based on the S-V approach	Unitless	McKew et al. (2013)
<b>ETR<sub>RCII</sub>-E curve parameters</b>			
$ETR_{RCII}$	Absolute electron transport rate through RCII	$\text{mol e}^{-1} \text{s}^{-1}$	Schuback et al. (2016)
$E$	Actinic light irradiance	$\text{mol photons m}^{-2} \text{s}^{-1}$	
$\alpha$	Light utilization index under dim light	$(\text{mol e}^{-1} \text{s}^{-1}) (\mu\text{mol photons m}^{-2} \text{s}^{-1})^{-1}$	Platt et al. (1980)
$\beta$	Light inhibition index under high light caused PSII photoinhibition	$(\text{mol e}^{-1} \text{s}^{-1}) (\mu\text{mol photons m}^{-2} \text{s}^{-1})^{-1}$	Platt et al. (1980)
$ETR_{\text{max}}$	Maximum electron transport rate through RCII	$\text{mol e}^{-1} \text{s}^{-1}$	Platt et al. (1980)
$E_k$	Light saturation index	$\mu\text{mol photons m}^{-2} \text{s}^{-1}$	Platt et al. (1980)

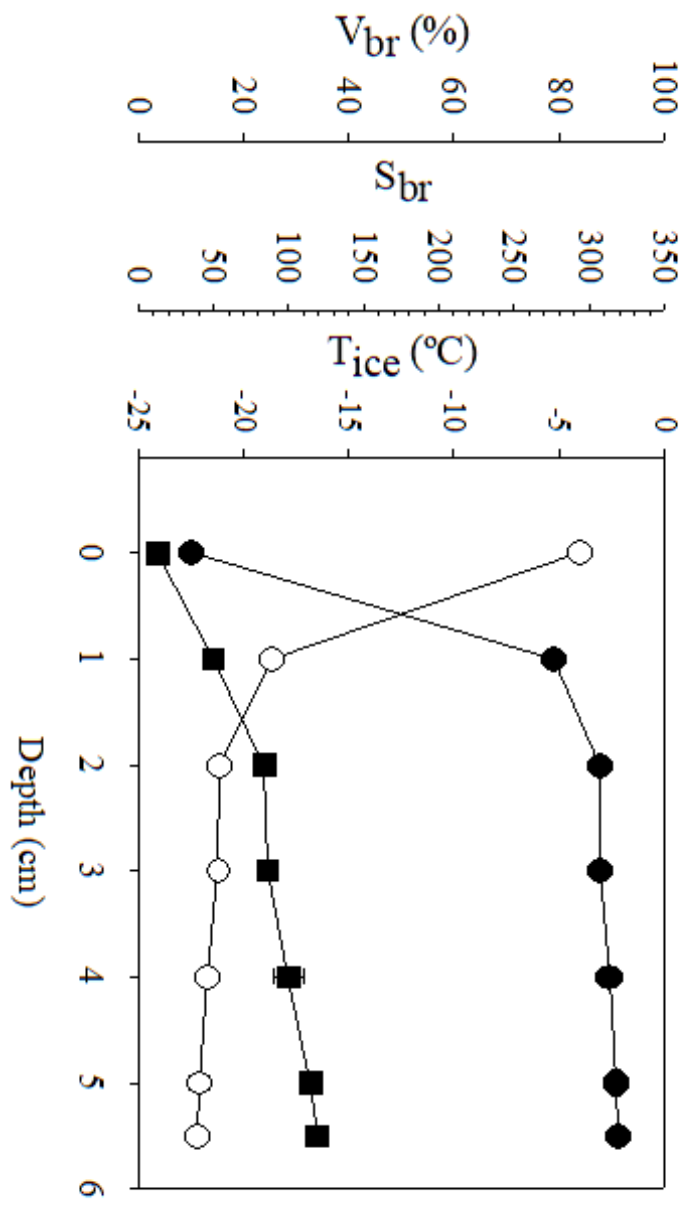
Table S1

<i>psbA</i>	
Forward primer	5'-AGAACCACCAAATACACCAGCAA-3'
Reverse primer	5'-TCCAAGCTGAGCACAAACATCTT-3'
Amplicon size	71
PCR condition	94 °C for 60 s; 40 cycles under 98 °C for 10 s, 62 °C for 60 s, and 72 °C for 60s
Baseline gene	Gene fragment of <i>Fragilariopsis cylindrus</i> from Antarctic sea ice <sup>*1</sup>
Reference	Krell et al. (2007)
<i>rbcL</i>	
Forward primer	5'-GATGATGARAAAYATTA ACTCW-3'
Reverse primer	5'-TAWGAACCTTTWACTTCWCC-3'
Amplicon size	113
PCR condition	94 °C for 60 s; 40 cycles under 98 °C for 10 s, 55 °C for 60 s, and 72 °C for 60s
Baseline gene	Gene fragment of <i>Thalassiosira weissflogii</i> (CCMP1336)
Reference	John et al. (2007); Endo et al. (2015)
720	*1: The isolate of <i>F.cylindrus</i> was obtained from Antarctic sea ice in the Weddel Sea in 1991
721	(Krell et al., 2007).



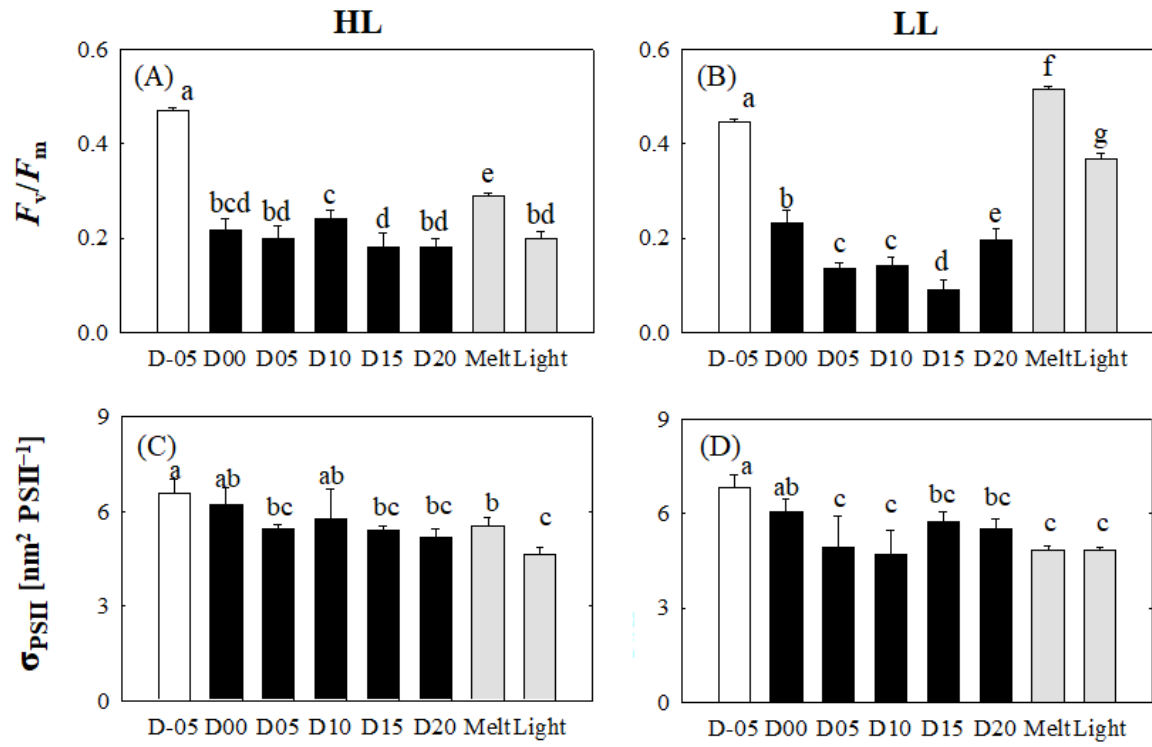
722

723 Fig. 1



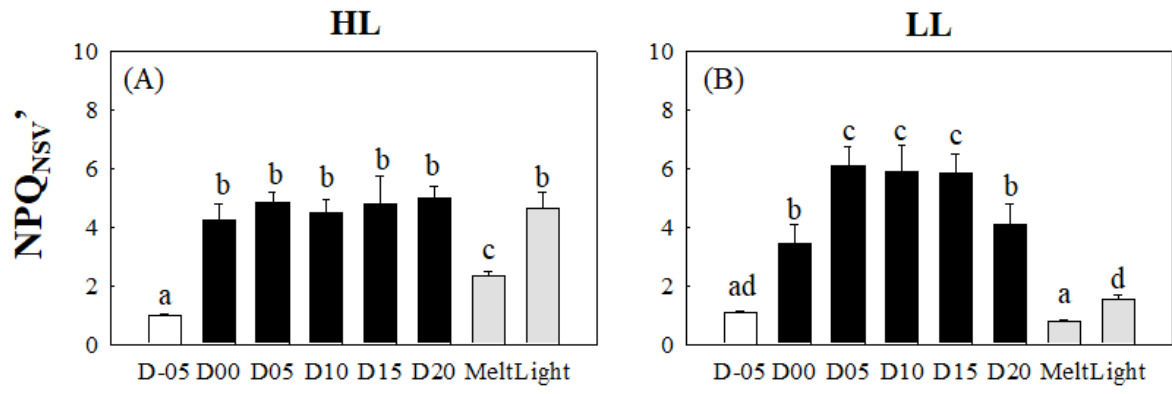
724

725 Fig.2



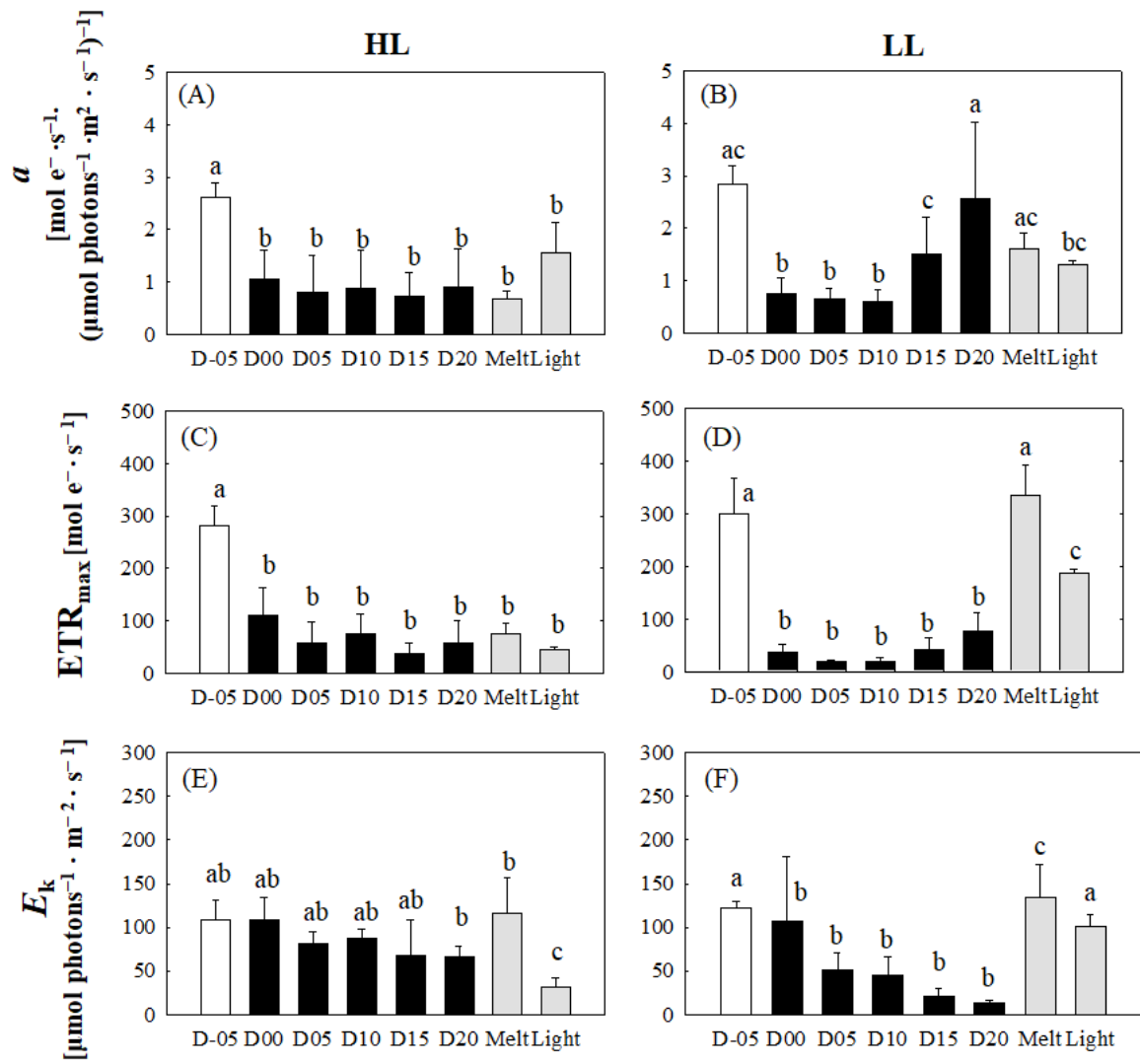
726

727 Fig. 3



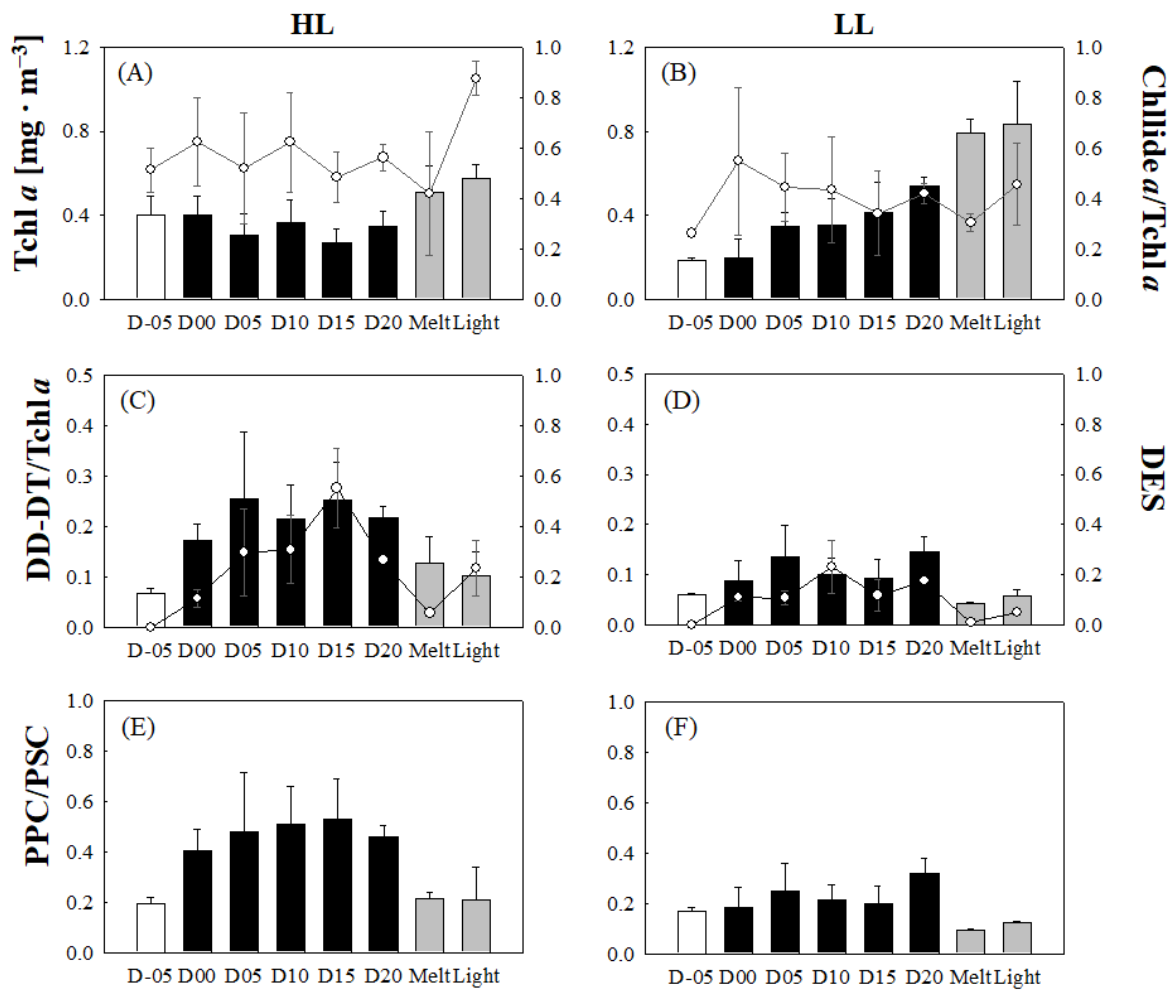
728

729 Fig. 4



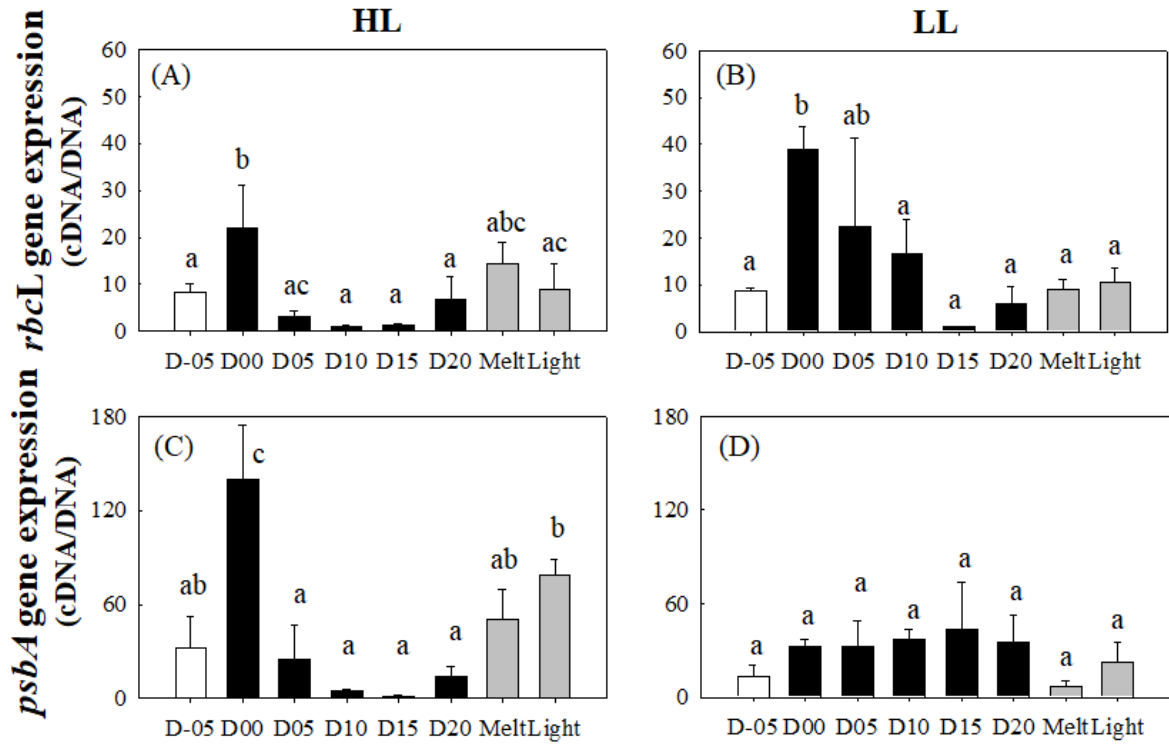
731

732 Fig. 5



733

734 Fig. 6



735

736 Fig. 7

737

738 Figure S2

739

740 **REFERENCES**

- 741 Allen, J.F. & Nilsson, A. 1997. Redox signalling and the structural basis of regulation of  
742 photosynthesis by protein phosphorylation. *Physiol. Plant.* 100:863–8.
- 743 Alou-Font, E., Mundy, C.-J., Roy, S., Gosselin, M. & Agustí, S. 2013. Snow cover affects ice  
744 algal pigment composition in the coastal Arctic Ocean during spring. *Mar. Ecol. Prog.*  
745 *Ser.* 474: 89–104.
- 746 Arrigo, K.R. 2014. Sea ice ecosystems. *Ann. Rev. Mar. Sci.* 6:439–67.
- 747 Arrigo, K.R. 2017. Sea ice as a habitat for primary producers. In Thomas, D.N. [Ed.] *Sea Ice*.  
748 3rd ed. Wiley Blackwell, pp. 352–369.
- 749 Arrigo, K.R., Mock, T. & Lizotte, M.P. 2010. Primary producers and sea ice. In Thomas,  
750 D.N. & Dieckmann, G.S. [Eds.] *Sea ice*. 2nd ed. Wiley Blackwell, pp. 283–326.
- 751 Arrigo, K.R. & van Dijken, G.L. 2003. Phytoplankton dynamics within 37 Antarctic coastal  
752 polynya systems. *J. Geophys. Res.* 108:3271.
- 753 Assmy, P., Ehn, J.K., Fernández-Méndez, M., Hop, H., Katlein, C., Sundfjord, A., Bluhm,  
754 K., Daase, M., Engel, A., Frasson, A., Granskog, M. A., Hudson, S, R., Kristiansen, S.,  
755 Nicolaus, M., Peeken, I., Renner, A. H. H., Spreen, G., Tatarek, A. & Wiktor, J. 2013.  
756 Floating ice-algal aggregates below melting arctic sea ice. *PLoS One.* 8:e76599.
- 757 Bailleul, B., Rogato, A., de Martino, A., Coesel, S., Cardol, P., Bowler, C., Falciatore, A. &  
758 Finazzi, G. 2010. An atypical member of the light-harvesting complex stress-related  
759 protein family modulates diatom responses to light. *Proc. Natl. Acad. Sci.* 107:18214–9.
- 760 Bernard, K., Gunther, L., Mahaffey, S., Qualls, K., Sugla, M., Saenz, B., Cossio, A., Walsh,  
761 J. & Reiss, C. 2018. The contribution of ice algae to the winter energy budget of juvenile  
762 Antarctic krill in years with contrasting sea ice conditions. *ICES J. Mar. Sci.* 1–11.
- 763 Boetius, A., Albrecht, S., Bakker, K., Bienhold, C., Felden, J., Fernandez-Mendez, M.,  
764 Hendricks, S., Katlein, C., Lalande, C., Krumpfen, T., Nicolaus, M., Peeken, I., Rabe, B.,

765 Rogacheva, A., Rybakova, E., Somavilla, R., Wenzhöfer, F. & RV Polarstern ARK27-3-  
766 Shipboard Science Party 2013. Export of algal biomass from the melting Arctic sea ice.  
767 *Science*. 339:1430–2.

768 Boetius, A., Anesio, A.M., Deming, J.W., Mikucki, J. & Rapp, J.Z. 2015. Microbial ecology  
769 of the cryosphere: sea ice and glacial habitats. *Nat. Rev. Microbiol.* 13:1–14.

770 Campbell, K., Mundy, C.J., Juhl, A.R., Dalman, L.A., Michel, C., Galley, R.J., Else, B.E.,  
771 Geilfus, N. X. & Rysgaard, S. 2019. Melt procedure affects the photosynthetic response  
772 of sea ice algae. *Front. Earth Sci.* 7:1–14.

773 Caron, L., Berkaloff, C., Duval, J.-C. & Jupin, H. 1987. Chlorophyll fluorescence transients  
774 from the diatom *Phaeodactylum tricornutum*: relative rates of cyclic phosphorylation  
775 and chlororespiration. *Photosynth. Res.* 11:131–9.

776 Cox, G.F.N. & Weeks, W.F. 1983. Equations for determining the gas and brine volumes in  
777 sea-ice samples. *J. Glaciol.* 29:306–16.

778 Devos, N., Ingouff, M., Loppes, R. & Matagne, R.F. 1998. Rubisco adaptation to low  
779 temperatures: a comparative study in psychrophilic and mesophilic unicellular algae. *J.*  
780 *Phycol.* 34:655–60.

781 D'Haene, S.E., Sobotka, R., Bučinská, L., Dekker, J.P. & Komenda, J. 2015. Interaction of  
782 the PsbH subunit with a chlorophyll bound histidine 114 of CP47 is responsible for the  
783 red 77 K fluorescence of Photosystem II. *Biochim. Biophys. Acta* 1847: 1327–34.

784 Domingues, N., Matos, A.R., da Silva, J.M. & Cartaxana, P. 2012. Response of the diatom  
785 *Phaeodactylum tricornutum* to photooxidative stress resulting from high light exposure.  
786 *PLoS One.* 7:1–6.

787 Danon, A. & Mayfield, S.P.Y. 1991. Light regulated translational activators: identification of  
788 chloroplast gene specific mRNA binding proteins. *EMBO J.* 10: 3993–4001.

789 Eiken, H. 2009. Ice sampling and basic ice core analysis. *In* Eiken, H., Gradinger, R.,

- 790 Salganek, M., Shirasawa, K., Perovich, D. & Leppäranta, M. [Eds.] *Field Techniques for*  
791 *Sea Ice Research*. University of Alaska Press, pp. 117–140.
- 792 Endo, H., Sugie, K., Yoshimura, T. & Suzuki, K. 2015. Effects of CO<sub>2</sub> and iron availability  
793 on *rbcL* gene expression in Bering Sea diatoms. *Biogeosciences*. 12:2247–59.
- 794 Endo, H., Yoshimura, T., Kataoka, T. & Suzuki, K. 2013. Effects of CO<sub>2</sub> and iron  
795 availability on phytoplankton and eubacterial community compositions in the northwest  
796 subarctic Pacific. *J. Exp. Mar. Bio. Ecol.* 439:160–75.
- 797 Ensminger, I., Busch, F. & Huner, N.P.A. 2006. Photostasis and cold acclimation: Sensing  
798 low temperature through photosynthesis. *Physiol. Plant.* 126:28–44.
- 799 Falkowski, P.G. & Owens, T.G. 1980. Light-shade adaptation: Two Strategies in marine  
800 phytoplankton. *Plant Physiol.* 66:592–5.
- 801 Falkowski, P.G. & Raven, J.A. 2013. *Aquatic Photosynthesis*. 2nd ed. Princeton University  
802 Press, 484 pp.
- 803 Fernández-Méndez, M., Katlein, C., Rabe, B., Nicolaus, M., Peeken, I., Bakker, K., Flores,  
804 H. & Boetius, A. 2015. Photosynthetic production in the central Arctic Ocean during the  
805 record sea-ice minimum in 2012. *Biogeosciences*. 12:3525–49.
- 806 Fernández-Méndez, M., Wenzhöfer, F., Peeken, I., Sørensen, H.L., Glud, R.N. & Boetius, A.  
807 2014. Composition, buoyancy regulation and fate of ice algal aggregates in the Central  
808 Arctic Ocean. *PLoS One*. 9:e107452.
- 809 Fiedor, L., Stašiek, M., Myśliwa-Kurdziel, B. & Strzałka, K. 2003. Phytol as one of the  
810 determinants of chlorophyll interactions in solution. *Photosynth. Res.* 78: 47–57.
- 811 Galindo, V., Gosselin, M., Lavaud, J., Mundy, C.J., Else, B., Ehn, J., Babin, M. & Rysgaard,  
812 S. 2017. Pigment composition and photoprotection of Arctic sea ice algae during spring.  
813 *Mar. Ecol. Prog. Ser.* 585:49–69.
- 814 Garrison, D.L. & Buck, K.R. 1986. Organism losses during ice melting: a serious bias in sea

815 ice community studies. *Polar Biol.* 6:237–9.

816 Goss, R. & Jakob, T. 2010. Regulation and function of xanthophyll cycle-dependent  
817 photoprotection in algae. *Photosynth. Res.* 106:103–22.

818 Goss, R. & Lepetit, B. 2015. Biodiversity of NPQ. *J. Plant Physiol.* 172:13–32.

819 Horner, R.A. 1985. *Sea Ice Biota*. CRC PRESS, 215 pp.

820 Huner, N.P.A., Öquist, G. & Sarhan, F. 1998. Energy balance and acclimation to light and  
821 cold. *Trends Plant Sci.* 3:224–30.

822 Jeffrey, S.W. & Hallegraeff, G.M. 1987. Chlorophyllase distribution in ten classes of  
823 phytoplankton: a problem for chlorophyll analysis. *Mar. Ecol. Prog. Ser.* 35:293–304.

824 John, D.E., Patterson, S.S. & Paul, J.H. 2007. Phytoplankton-group specific quantitative  
825 polymerase chain reaction assays for RuBisCO mRNA transcripts in seawater. *Mar.*  
826 *Biotechnol.* 9:747–59.

827 Katayama, T. & Taguchi, S. 2013. Photoprotective responses of ice algal community in  
828 Saroma-Ko Lagoon, Hokkaido, Japan. *Polar Biol.* 36:1431–9.

829 Katlein, C., Fernández-Méndez, M., Wenzhöfer, F. & Nicolaus, M. 2015. Distribution of  
830 algal aggregates under summer sea ice in the Central Arctic. *Polar Biol.* 38:719–31.

831 Kennedy, F., Martin, A., Bowman, J.P., Wilson, R. & McMinn, A. 2019. Dark metabolism: a  
832 molecular insight into how the Antarctic sea-ice diatom *Fragilariopsis cylindrus*  
833 survives long-term darkness. *New Phytologist* 223: 675–91.

834 Kennedy, F., McMinn A. & Martin A. 2012. Effect of temperature on the photosynthetic  
835 efficiency and morphotype of *Phaeocystis antarctica*. *J. Exp. Mar. Biol. Ecol.* 429:  
836 7–14.

837 Kohlbach, D., Lange, B.A., Schaafsma, F.L., David, C., Vortkamp, M., Graeve, M., van  
838 Franeker, J.A., Krumpfen, T. & Flores, H. 2017. Ice algae-produced carbon is critical for

839 overwintering of Antarctic krill *Euphausia superba*. *Front. Mar. Sci.* 4:1–16.

840 Kolber, Z.S., Prášil, O. & Falkowski, P.G. 1998. Measurements of variable chlorophyll  
841 fluorescence using fast repetition rate techniques: Defining methodology and  
842 experimental protocols. *Biochim. Biophys. Acta.* 1367:88–106.

843 Krell, A., Funck, D., Plettner, I., John, U. & Dieckmann, G. 2007. Regulation of proline  
844 metabolism under salt stress in the psychrophilic diatom *Fragilariopsis cylindrus*  
845 (Bacillariophyceae). *J. Phycol.* 43:753–62.

846 Kropuenske, L.R., Mills, M.M., van Dijken, G.L., Alderkamp, A., Mine Berg, G., Robinson,  
847 D.H., Welschmeyer, N.A. & Arrigo, K. R. 2010. Strategy and rates of photoacclimation  
848 in two major phytoplankton taxa: *Phaeocystis antarctica* (haptophyta) and *Fragilariopsis*  
849 *cylindrus* (Bacillariophyceae). *J. Phycol.* 46:1138–51.

850 Kropuenske, L.R., Mills, M.M., van Dijken, G.L., Bailey, S., Robinson, D.H., Welschmeyer,  
851 N.A. & Arrigo, K.R. 2009. Photophysiology in two major southern ocean phytoplankton  
852 taxa: Photoprotection in *Phaeocystis antarctica* and *Fragilariopsis cylindrus*. *Limnol.*  
853 *Ocean.* 54:1176–96.

854 Kuczynska, P., Jemiola-Rzeminska, M. & Strzalka, K. 2015. Photosynthetic pigments in  
855 diatoms. *Mar. Drugs.* 13:5847–81.

856 Lacour, T., Larivière, J., Ferland, J., Bruyant, F., Lavaud, J. & Babin, M. 2018. The role of  
857 sustained photoprotective non-photochemical quenching in low temperature and high  
858 light acclimation in the bloom-forming Arctic diatom *Thalassiosira gravida*. *Front.*  
859 *Mar. Sci.* 5:1–16.

860 Lavaud, J., Rousseau, B. & Etienne, A.-L. 2002. In diatoms, a transthylakoid proton gradient  
861 alone is not sufficient to induce a non-photochemical fluorescence quenching. *FEBS*  
862 *Lett.* 523:163–6.

863 Lazár, D., Ilík, P., Kruk, J., Strzalka, K. & Nauš, J. 2005. A theoretical study on effect of the

864 initial redox state of cytochrome *b*<sub>559</sub> on maximal chlorophyll fluorescence level ( $F_M$ ):  
865 Implications for photoinhibition of photosystem II. *J. Theor. Biol.* 233:287–300.

866 Legendre, L., Ackley, S. F., Dieckmann, G. S., Gulliksen, B., Horner, R., Hoshiai, T.,  
867 Melnikov, I. A., Reeburgh, W. S., Spindler, M. & Sullivan, C. W. 1992. Ecology of sea  
868 ice biota. *Polar Biol.* 12:429–44.

869 LeGresley, M. & McDermott, G. 2010. Counting chamber methods for quantitative  
870 phytoplankton analysis—Haemocytometer, Palmer-Maloney cell and Sedwick-rafter cell.  
871 In Karlson, B., Cusack, C. & Bresnan, E. [Eds.] *Microscopic and Molecular Methods*  
872 *for Quantitative Phytoplankton Analysis*. UNESCO, pp. 25–30.

873 Lepetit, B., Volke, D., Gilbert, M., Wilhelm, C. & Goss, R. 2010. Evidence for the existence  
874 of one antennae-associated. lipid-dissolved and two protein-bound pools of  
875 diadinoxanthin cycle pigments in diatoms. *Plant Physiol.* 154: 1905–1920.

876 Lepetit, B., Strum, S., Rogato, A., Gruber, A., Sachse, M., Falciatore, A., Kroth, P.G. &  
877 Lavaud, J. 2013. High light acclimation in the secondary plastids containing diatom  
878 *Phaeodactylum tricorutum* is triggered by the redox state of the plastoquinone pool.  
879 *Plant Physiol.* 161: 853–865.

880 Lizotte, M.P. 2001. The contributions of sea ice algae to Antarctic marine primary  
881 production. *Am. Zool.* 41:57–73.

882 Loose, B., Miller, L.A., Elliott, S. & Papakyriakou, T. 2011. Sea ice biogeochemistry and  
883 material transport across the frozen interface. *Oceanography.* 24:202–18.

884 Lyon, B. & Mock, T. 2014. Polar microalgae: New approaches towards understanding  
885 adaptations to an extreme and changing environment. *Biology.* 3:56–80.

886 Maccario, L., Sanguino, L., Vogel, T.M. & Larose, C. 2015. Snow and ice ecosystems: Not  
887 so extreme. *Res. Microbiol.* 166:782–95.

888 MacIntyre, H.L., Kana, T.M., Anning, T. & Geider, R.J. 2002. Photoacclimation of

889 photosynthesis irradiance response curves and photosynthetic pigments in microalgae  
890 and cyanobacteria. *J. Phycol.* 38: 17–38.

891 Malnoë, P., Mayfield, S.P. & Rochaix, J.-D. 1988. Comparative analysis of the biogenesis of  
892 photosystem II in the wild-type and Y-1 mutant of *Chlamydomonas reinhardtii*. *J. Cell*  
893 *Biol.* 106: 609–616.

894 Martin, A., Anderson, M.J., Thorn, C., Davy, S.K. & Ryan, K.G. 2011. Response of sea-ice  
895 microbial communities to environmental disturbance: An *in situ* transplant experiment in  
896 the Antarctic. *Mar. Ecol. Prog. Ser.* 424:25–37.

897 Maxwell, D.P., Laudenbach, D.E. & Huner, N. 1995. Redox regulation of light-harvesting  
898 complex II and *cab* mRNA abundance in *Dunaliella salina*. *Plant Physiol.* 109:787–95.

899 McKew, B.A., Davey, P., Finch, S.J., Hopkins, J., Lefebvre, S.C., Metodiev, M. V.,  
900 Oxborough, K., Raines, C. A., Lawson, T. & Geider, R. J. 2013. The trade-off between  
901 the light-harvesting and photoprotective functions of fucoxanthin-chlorophyll proteins  
902 dominates light acclimation in *Emiliana huxleyi* (clone CCMP 1516). *New Phytol.*  
903 200:74–85.

904 McMinn, A. 2017. Ice Acidification: A review of the effects of ocean acidification on sea ice  
905 microbial communities. *Biogeosciences.* 14:3927–35.

906 McMinn, A., Hattori, H., Hirawake, T. & Iwamoto, A. 2008. Preliminary investigation of  
907 Okhotsk Sea ice algae; taxonomic composition and photosynthetic activity. *Polar Biol.*  
908 31:1011–5.

909 McMinn, A. & Hegseth, E.N. 2004. Quantum yield and photosynthetic parameters of marine  
910 microalgae from the southern Arctic Ocean, Svalbard. *J. Mar. Biol. Assoc. United*  
911 *Kingdom.* 84:865–71.

912 McMinn, A., Muller, M.N., Martin, A. & Ryan, K.G. 2014. The response of Antarctic sea ice  
913 algae to changes in pH and CO<sub>2</sub>. *PLoS One.* 9:e86984.

- 914 McMinn, A., Pankowski, A., Ashworth, C., Bhagooli, R., Ralph, P. & Ryan, K. 2010. In situ  
915 net primary productivity and photosynthesis of Antarctic sea ice algal, phytoplankton  
916 and benthic algal communities. *Mar. Biol.* 157:1345–56.
- 917 Melnikov, I.A. & Bondarchuk, L.L. 1987. Ecology of mass accumulations of colonial diatom  
918 algae under drifting Arctic ice. *Oceanology.* 27:233–6.
- 919 Michel, C., Ingram, R.G. & Harris, L.R. 2006. Variability in oceanographic and ecological  
920 processes in the Canadian Arctic Archipelago. *Prog. Oceanogr.* 71:379–401.
- 921 Mikkelsen, D.M. & Witkowski, A. 2010. Melting sea ice for taxonomic analysis: A  
922 comparison of four melting procedures. *Polar Res.* 29:451–4.
- 923 Miller, L.A., Fripiat, F., Else, B.G.T., Bowman, J.S., Brown, K.A., Collins, R.E., Ewert, M.,  
924 Frasson, A., Gosselin, M., Lannuzel, D., Meiners, K. M., Michel, C., Nishioka, J.,  
925 Nomura, D., Papadimitrou, S., Russell, L. M., Sørensen, L. L., Thomas, D. N., Tison, J.-  
926 L., van Leeuwe, M., Vancoppenolle, M., Wolff, E. & Zhou, J. 2015. Methods for  
927 biogeochemical studies of sea ice: The state of the art, caveats, and recommendations.  
928 *Elem. Sci. Anthr.* 3:000038.
- 929 Mock, T. & Hoch, N. 2005. Long-term temperature acclimation of photosynthesis in steady-  
930 state cultures of the polar diatom *Fragilariopsis cylindrus*. *Photosynth. Res.* 85:307–17.
- 931 Morgan-Kiss, R.M., Priscu, J.C., Pockock, T., Gudynaite-Savitch, L. & Huner, N.P.A. 2006.  
932 Adaptation and acclimation of photosynthetic microorganisms to permanently cold  
933 environments. *Microbiol. Mol. Biol. Rev.* 70:222–52.
- 934 Moteki, M., Odate, T., Hosie, G.W., Takahashi, K.T., Swadling, K.M. & Tanimura, A. 2017.  
935 Ecosystem studies in the Indian Ocean sector of the Southern Ocean undertaken by the  
936 training vessel *Umitaka-maru*. *Polar Sci.* 12:1–4.
- 937 Mulo, P., Sakurai, I & Aro, E.-M. 2012. Strategies for *psbA* gene expression in  
938 cyanobacteria, green algae and higher plants: From transcription to PSII repair. *Biochim.*

939 *Biophys. Acta* 187: 247–257.

940 Nymark, M., Valle, K.C., Hancke, K., Winge, P., Andresen, K., Johnsen, G., Bones, A.M. &  
941 Brembu, T. 2013. Molecular and photosynthetic responses to prolonged darkness and  
942 subsequent acclimation to re-illumination in the diatom *Phaeodactylum tricorutum*.  
943 *PLoS One*. 8:e58722.

944 Öquist, G. & Huner, N.P.A. 2003. Photosynthesis of overwintering evergreen plants. *Annu.*  
945 *Rev. Plant Biol.* 54:329–55.

946 Oxborough, K. & Baker, N.R. 1997. Resolving chlorophyll *a* fluorescence images of  
947 photosynthetic efficiency into photochemical and non-photochemical components -  
948 Calculation of *qP* and *Fv'/Fm'* without measuring *Fo'*. *Photosynth. Res.* 54:135–42.

949 Petrich, C. & Eicken, H. 2017. Overview of sea ice growth and properties. In Thomas, D.N.  
950 [Ed.] *Sea Ice*. 3rd ed. Wiley Blackwell, pp. 1–41.

951 Petrou, K., Hill, R., Brown, C.M., Campbell, D.A., Doblin, M.A. & Ralph, P.J. 2010. Rapid  
952 photoprotection in sea-ice diatoms from the East Antarctic pack ice. *Limnol. Oceanogr.*  
953 55:1400–7.

954 Pfannschmidt, T. 2003. Chloroplast redox signals: How photosynthesis controls its own  
955 genes. *Trends Plant Sci.* 8:33–41.

956 Platt, T., Gallegos, C.L. & Harrison, W.G. 1980. Photoinhibition of photosynthesis in natural  
957 assemblages of marine phytoplankton. *J. Mar. Res.* 38:687–701.

958 Price, N.M., Harrison, G.I., Hering, J.G., Hudson, R.J., Nirel, P.M. V., Palenik, B. & Morel,  
959 F.M.M. 1989. Preparation and chemistry of the artificial algal culture medium Aquil.  
960 *Biol. Oceanogr.* 6:443–61.

961 Ralph, P.J. & Gademann, R. 2005. Rapid light curves: A powerful tool to assess  
962 photosynthetic activity. *Aquat. Bot.* 82:222–37.

963 Ralph, P.J., McMinn, A., Ryan, K.G. & Ashworth, C. 2005. Short-term effect of temperature

964 on the photokinetics of microalgae from the surface layers of Antarctic pack ice. *J.*  
965 *Phycol.* 41:763–9.

966 Ralph, P.J., Ryan, K.G., McMinn, A. & Fenton, G. 2007. Melting out of sea ice causes  
967 greater photosynthetic stress in algae than freezing in. *J. Phycol.* 43: 948–56.

968 Riebesell, U., Schloss, I. & Smetacek, V. 1991. Aggregation of algae released from melting  
969 sea ice: implications for seeding and sedimentation. *Polar Biol.* 11:239–48.

970 Rintala, J.M., Piiparinen, J., Blomster, J., Majaneva, M., Müller, S., Uusikivi, J. & Autio, R.  
971 2014. Fast direct melting of brackish sea-ice samples results in biologically more  
972 accurate results than slow buffered melting. *Polar Biol.* 37:1811–22.

973 Rosenbach-Belkin, V., Fisher, J.R.E. & Scherz, A. 1991. Effects of nonexitonic interaction  
974 among the paired molecules on the Q<sub>y</sub> transition of bacteriochlorophyll dimers.  
975 Applications to the primary electron donors P-860 and P-960 in bacterial reaction  
976 centers. *J. Am. Chem. Soc.* 113: 676–678.

977 Ryan, K.G., Tay, M.L., Martin, A., McMinn, A. & Davy, S.K. 2011. Chlorophyll  
978 fluorescence imaging analysis of the responses of Antarctic bottom-ice algae to light and  
979 salinity during melting. *J. Exp. Mar. Bio. Ecol.* 399:156–61.

980 Sakshaug, E. & Slagstad, D. 1991. Light and productivity of phytoplankton in polar marine  
981 ecosystems: a physiological view. *Polar Res.* 10:69–86.

982 Satoh, H., Yamaguchi, Y., Watanabe, K., Tanimura, A., Fukuchi, M. & Aruga, Y. 1989.  
983 Photosynthetic nature of ice algae and their contribution to the primary production in  
984 Lagoon Saroma Ko, Hokkaido, Japan. *Proc. NIPR Symp. Polar Biol.* 2:1–8.

985 Schuback, N., Flecken, M., Maldonado, M.T. & Tortell, P.D. 2016. Diurnal variation in the  
986 coupling of photosynthetic electron transport and carbon fixation in iron-limited  
987 phytoplankton in the NE subarctic Pacific. *Biogeosciences.* 13:1019–35.

988 Schwarz, V., Andosch, A., Geretschläger, A., Affenzeller, M. & Lütz-Meindl, U. 2017.

- 989 Carbon starvation induces lipid degradation via autophagy in the model alga  
990 *Micrasterias*. *J. Plant Physiol.* 208:115–27.
- 991 Smith, W.O. & Nelson, D.M. 1986. Importance of ice edge phytoplankton production in the  
992 Southern Ocean. *Bioscience.* 36:251–7.
- 993 Suggett, D.J., Moore, C.M., Hickman, A.E. & Geider, R.J. 2009. Interpretation of fast  
994 repetition rate (FRR) fluorescence: Signatures of phytoplankton community structure  
995 versus physiological state. *Mar. Ecol. Prog. Ser.* 376:1–19.
- 996 Suggett, D.J., Prášil, O. & Borowitzka, M.A. 2011. *Chlorophyll a Fluorescence in Aquatic  
997 Sciences: Methods and Applications*. Springer, New York, US, 323 pp.
- 998 Suzuki, K., Kamimura, A. & Hooker, S.B. 2015. Rapid and highly sensitive analysis of  
999 chlorophylls and carotenoids from marine phytoplankton using ultra-high performance  
1000 liquid chromatography (UHPLC) with the first derivative spectrum chromatogram  
1001 (FDSC) technique. *Mar. Chem.* 176:96–109.
- 1002 Syvertsen, E.E. 1991. Ice algae in the Barents Sea: types of assemblages, origin, fate and role  
1003 in the ice-edge phytoplankton bloom. *Polar Res.* 10:277–88.
- 1004 Szechynska-Hebda, M., Kruk, J., Gorecka, M., Karpinska, B. & Karpinski, S. 2010. Evidence  
1005 for light wavelength-specific photoelectrophysiological signaling and memory of excess  
1006 light episodes in *Arabidopsis*. *Plant Cell Online.* 22:2201–18.
- 1007 Taguchi, S., Saito, H., Shirasawa, K. & Hattori, H. 1997. Vertical flux of ice algal cells  
1008 during the ice melting and breaking periods in Saroma Ko Lagoon, Hokkaido, Japan.  
1009 *Proc. NIPR Symp. Polar Biol.* 10:56–65.
- 1010 Ting, C.S. & Owens, T.G. 1993. Photochemical and nonphotochemical fluorescence  
1011 quenching processes in the diatom *Phaeodactylum tricorutum*. *Plant Physiol.*  
1012 101:1323–30.
- 1013 van Leeuwe, M.A., Tedesco, L., Arrigo, K.R., Assmy, P., Campbell, K., Meiners, K.M.,

- 1014 Rintala, J.-M., Selz, V., Thomas, D. N. & Stefel, J. 2018. Microalgal community  
1015 structure and primary production in Arctic and Antarctic sea ice: A synthesis. *Elem Sci*  
1016 *Anth.* 6: 4.
- 1017 Yamamoto, S., Michel, C., Gosselin, M., Demers, S., Fukuchi, M. & Taguchi, S. 2014.  
1018 Photosynthetic characteristics of sinking microalgae under the sea ice. *Polar Sci.* 8:385–  
1019 96.
- 1020 Wood, A.M., Everroad, R.C. & Wingard, L.M. 2005. Measuring growth rates in microalgal  
1021 culture. In Andersen, R.A. [Ed.] *Algal Culturing Techniques*. Elsevier, Amsterdam,  
1022 Netherland, 269–285.
- 1023 Yan, D., Endo, H. & Suzuki, K. 2019. Increased temperature benefits growth and  
1024 photosynthetic performance of the sea ice diatom *Nitzschia cf. neglecta*  
1025 (Bacillariophyceae) isolated from Saroma Lagoon, Hokkaido, Japan. *J. Phycol.* 55:  
1026 700–13.
- 1027 Yoshida, K., Endo, H., Lawrenz, E., Isada, T., Hooker, S.B., Prášil, O. & Suzuki, K. 2018.  
1028 Community composition and photophysiology of phytoplankton assemblages in coastal  
1029 Oyashio waters of the western North Pacific during early spring. *Estuar. Coast. Shelf*  
1030 *Sci.* 212: 80–94.
- 1031 Young, J.N., Goldman, J.A.L., Kranz, S.A., Tortell, P.D. & Morel, F.M.M. 2015. Slow  
1032 carboxylation of Rubisco constrains the rate of carbon fixation during Antarctic  
1033 phytoplankton blooms. *New Phytol.* 205:172–81.